DEUTSCHES ELEKTRONEN-SYNCHROTRON DESY

DESY SR-86-03
May 1986

TIME AND SPECTRALLY RESOLVED FLUORESCENCE OF Cl_2 AND ArCl IN Cl_2 DOPED Ar UNDER STATE SELECTIVE PULSED PHOTOEXCITATION WITH SYNCHROTRON RADIATION

by

T. Möller, B. Jordan, G. Zimmerer

II. Institut für Experimentalphysik, Universität Hamburg

D. Haaks

FB Physikalische Chemie der Universität - GHS Wuppertal -

J. le Calvé

Centre d'Etudes Nucléaires de Saclay - IRDI - Département de Physico-Chimie

M.-C. Castex

Laboratoire des Interactions Moléculaires et des Hautes Pressions du C.N.R.S. - Centre Universitaire Paris-Nord -

ISSN 0723-7979

NOTKESTRASSE 85 · 2 HAMBURG 52

To be sure that your preprints are promptly included in the
HIGH ENERGY PHYSICS INDEX ,
send them to the following address (if possible by air mail) :

DESY
Bibliothek
Notkestrasse 85
2 Hamburg 52
Germany

DESY SR-86-03
May 1986

TIME AND SPECTRALLY RESOLVED FLUORESCENCE OF Cl_2 AND ArCl IN Cl_2 DOPED Ar UNDER STATE SELECTIVE PULSED PHOTOEXCITATION WITH SYNCHROTRON RADIATION

Thomas MÖLLER (1), Bernhard JORDAN (1), Georg ZIMMERER (1), Dieter HAAKS (2), Jacques LE CALVÉ (3), Marie-Claude CASTEX (4)

(1) II Institut für Experimentalphysik der Universität Hamburg, D-2000 HAMBURG 50 - GERMANY

(2) FB Physikalische Chemie der Universität - GHS Wuppertal - D-5600 WUPPERTAL - GERMANY

(3) Centre d'Etudes Nucléaires de Saclay - IRDI - Département de Physico-Chimie - 91191 GIF sur YVETTE - FRANCE

and

(4) Laboratoire des Interactions Moléculaires et des Hautes Pressions du C.N.R.S. - Centre Universitaire Paris-Nord - 93430 VILLETANEUSE - FRANCE

submitted to: Zeitschrift für Physik

ISSN 0723-7979

Abstract

Synchrotron Radiation is used to selectively excite chlorine and Cl_2 doped argon in the VUV region. Stationary fluorescence and excitation spectra of $1^1\Sigma_u^+$, $2^1\Sigma_u^+$ and $2^3\Pi_g$ Cl_2 states and of the ArCl (B-X) transition are obtained. The excitation threshold of ArCl (B) in Ar/Cl_2 system is found to be 1285 ± 5 Å. The formation of $ArCl^*$ and $Cl_2(2^3\Pi g)$ is discussed in terms of recent potential curves data. A detailed time resolved study is reported which allows us to determine precisely the radiative lifetime of ArCl(B) state (5.2 ns) and numerous kinetic parameters of this system, to estimate the C state energy and to discuss the relaxation and mixing process of the ArCl(B) and (C) states. A two ladder multilevel kinetic model is described which accounts for the experimental results and shows the difficulty of studying this particular ArCl system compared to the closely related XeCl and KrCl ones.

Code PACS : 3490, 3320N, 8220K.

1 - Introduction

Rare gas monohalides with their weakly bound van der Waals ground state are not stable but exist only in short lived electronically excited states. In the heavier molecules, the lowest bound excited states (B,C,D) are of ionic nature (1-3). The molecules are produced in mixtures of rare gases with halogen donors in elementary reactions of electronically excited or ionized species (4). The main source of information on the electronic structure is fluorescence which is of the bound-free type. The dominating transition is the $B \rightarrow X$ transition, however, $C \rightarrow A$ and $D \rightarrow X$ can also be observed (4). Some rare gas monohalides play an important role as laser molecules in high power UV excimer lasers. Therefore, besides the spectroscopic properties of the emitting states, the dynamical aspects of formation, relaxation and decay of these molecules are the subject of several investigations.

In rare gas monohalides laser systems of the discharge type (5) or with e^- beam excited experiments (6,7), the reaction kinetics are extremely complicated by the superposition of various processes. Therefore it is highly desirable to study the kinetic processes under well defined primary excitation conditions. This was first done successfully, e.g., with flowing afterglow techniques, in which the elementary reactions of rare gas (Rg) metastables with the halogen donor were studied (8-10). Information about dynamical processes was obtained from the

measurement of relative intensities of competing fluorescence channels.

In general, most reliable data on dynamical processes (like rate constants, lifetimes, etc ...) can be extracted from time resolved fluorescence spectra following state selective primary excitation. True state selective excitation of rare gas monohalides is difficult. In most cases, the molecules are produced in an elementary reaction in a broad, athermal vibrational distribution (11). Moreover, the B and the C state being nearly degenerate, both excited states are produced at the same time. Only in two cases ($XeCl^*$ and $XeBr^*$), state selective excitation of various vibrational levels of the B state was possible up to now by exciting ground state molecules with a laser (12-13).

Synchrotron Radiation (SR), combining the advantages of a pulsed and VUV tunable source for state selective excitation with time and spectrally resolved fluorescence spectroscopy, is particularly well suited for these studies.

Our preliminary work on Kr/Cl_2 (and Ar/Cl_2) was undertaken at the fluorescence experimental station of the storage ring ACO at ORSAY (14,15). Our further studies have been carried out with considerably increased sensitivity and time resolution at the Synchrotron Radiation Laboratory (HASYLAB) of DESY/HAMBURG (16-18).

In our first papers (14,15) we unambiguously showed that not only collisions of the type $Rg^* + Cl_2 \rightarrow RgCl^* + Cl$ (Rg : Ar, Kr) but also $Rg + Cl_2^* \rightarrow RgCl^* + Cl$ lead to the formation of the monohalides. The several vibrational progressions of Cl_2 in the VUV (18,19,20) make it feasible to tune quasicontinuously the

entrance energy of the reaction over a wide range. This new formation channel (from Cl_2) was especially exploited in our work with Synchrotron Radiation. In a recent paper, we have reported reliable values of kinetic parameters, mainly in XeCl and KrCl systems, and have been interested in the evaluation of the energy difference and ordering of the B and C states (21). This is indeed of crucial importance for the dynamical decay properties of the collisionaly mixed B and C states in laser systems.

This paper is focused more precisely on ArCl where primary Cl_2 excitation offers the unique opportunity to scan through the threshold of the formation reaction and to produce vibrationally relaxed B state molecules. This simplifies the analysis of kinetic data considerably. Excitation at higher energies leads to $ArCl^*$ in a broad vibrational distribution (high v') of the B and the C state. Then the influence of the collisional mixing of both states in the de-excitation process can be deduced.

A special feature of the Ar + Cl_2 reaction is the fact that not only $ArCl^*$ but also Cl_2^* ($2^3\Pi_g$) molecules are formed which lead to the Cl_2 laser emission at 2580 Å. The nomenclature for the Cl_2 states is in accordance with ref. (18,19). In sec. 3, stationary time integrated fluorescence and excitation spectra of $ArCl^*$ and Cl_2^* emissions are presented. The formation mechanisms both of $ArCl^*$ and Cl_2 ($2^3\Pi_g$) following primary Cl_2^* excitation are discussed. In the threshold region, the Cl_2^* ($2^1\Sigma_u^+$) state is the dominating primary state. Most probably, collision induced intersystem crossing leads to Cl_2^* ($2^3\Pi_g$) formation. $ArCl^*$ production is at least partly due to a complicated pathway with two steps, (i) intramolecular relaxation $2^1\Sigma_u^+ \rightarrow 1^1\Sigma_u^+$ via diabatic

crossing of two potential curves, followed by (ii) an elementary reaction of the type $Ar + (Cl^+ Cl^-)^* \rightarrow (Ar^+ Cl^-)^* + Cl$.

In sec. 4, detailed time resolved measurements are presented. Special care is taken on the overlap at 1750 Å of both ArCl (B-X) and $Cl_2(1^1\Sigma_u^+ \rightarrow X)$ emission signals. Excitation close to the threshold yields the dynamical properties of the vibrationally relaxed ArCl (B) state. Higher primary excitation leads to an estimation of the C state energy and information about B/C mixing process. The collisional two level mixing model, which correctly accounts for the results obtained in XeCl and KrCl system (21), is no longer valid for ArCl. A two ladder multilevel mixing and relaxation model is presented.

2 - Experiment

The experimental work reported here was carried out in the Synchrotron Radiation (SR) laboratory HASYLAB at DESY, Hamburg. The stationary and part of the time resolved spectra were obtained at an experimental station which is described elsewhere (16,22).

The partial pressures in the Ar/Cl_2 mixtures range between .5 torr and 10 torr (Cl_2) and between 50 torr and 600 torr (Ar). The gas mixtures were prepared in a Viton-sealed stainless-steel gas-handling system with a base pressure $< 10^{-7}$ torr. The gases were Matheson research grade (Cl_2) and Ar N47 (99.997 %) (l'Air Liquide).

The excimers were produced in a stainless steel gas cell via state-selective excitation of one of the components with SR. SR was dispersed with a 1 m VUV monochromator at a spectral resolution of 4 Å (fwhm). The exciting radiation was focused on

a point inside the gas cell. The spectral range of excitation was restricted by the transmission characteristics of the LiF windows to $\lambda > 1040$ Å. Fluorescence was analyzed at a right angle to the exciting beam with a .4 m Seya Namioka monochromator at a band pass of 12 Å. The fluorescence signal was detected with a solar blind type photomultiplier (stationary spectra) and with a Valvo XP 2020 Q photomultiplier (time resolved spectra) without any wavelength shifter.

The pulsed nature of SR is the basis for the time resolved experiments. At HASYLAB, SR consists of light flashes with a fwhm of $\sim$ 150 ps at a repetition rate between 1 MHz and 480 MHz. During our experiments, the SR source was operated with repetition rates of 40 MHz and of 20 MHz so that only time constants < 20 or 50 ns could be investigated.

The ultimate limit on time resolution in this experiment is set by the time characteristics of the detector. With appropriate deconvolution techniques, characteristic time constants down to 500 ps were measured with the Valvo XP 2020 Q. Single photon counting and timing was used to measure the decay rates of spectrally selected fluorescence bands (22,23). Analysis of the decay curves was performed with the aid of a computer program of Striker (24) which makes possible the fitting of the decay curves with up to three exponentials and which also includes different mathematical tests of the reliability and accuracy on the fits.

Another part of the time resolved experiments was carried out at the experimental station SUPERLUMI which is described elsewhere (25,26). SR was dispersed with a 2m VUV monochromator at a spectral resolution of 2 Å. Fluorescence was analysed with a VUV

toroidal grating monochromator at a band pass of 8 Å. The fluorescence signal was detected with a channel plate detector with an ultimate time resolution of $\sim$ 100 ps. Due to the high excitation intensity of this experimental station, the Ar pressure could be lowered to a few torr. The storage ring was operated at 1 MHz. Therefore, lifetimes longer than 50 ns were also accessible.

3 - Stationary fluorescence and excitation spectra

3-1) Results

Fig. 1 shows a fluorescence spectrum of 275 torr Ar doped with .3 % Cl_2. The system was not excited selectively but with the 0th order of the primary monochromator. The spectrum is not corrected for the transmission curve of LiF windows of the gas cell. The fluorescence originates in :

(i) bound-free type Ar_2^* fluorescence peaking at 1265 Å. (27)

(ii) $Cl_2^*(1^1\Sigma_u^+)$ emission containing both bound-bound and bound-free contributions, which extend from $\sim$ 1400 Å to $\sim$ 2000 Å. (18,19)

(iii) superimposed on (ii), the $B \rightarrow X$ fluorescence of $ArCl^*$ (4)

(iv) $Cl_2^*(2^3\Pi_g)$ emission with its maximum at 2580 Å (15,28)

The fluorescence is so complex that we were only able to understand it in satisfactory detail by performing spectral analyses of excitation as well as emission.

Fig. 2 shows selectively excited fluorescence spectra. In the upper part, Cl_2 was excited at 1180 Å. In the lower part, Ar was excited at 1066 Å ($Ar\ ^3P_1$). Under primary Cl_2 excitation, the two main decay channels are of comparable intensity. Under primary

Ar excitation, $ArCl^*$ emission dominates. We want to point out, however, that the spectral distribution is also a function of the total pressure conditions.

The particular role of the primarily excited state manifests itself most directly in the excitation spectra of the different radiative decay channels. Fig. 3 displays excitation spectra of the $ArCl^*$ emission and of $Cl_2(2^3\Pi_g)$ emission (upper curve). Characteristic excitation wavelengths are marked at the top of the figure. Only two Ar excitations are available below the LiF cut off, namely $Ar\,^3P_1$ and $^1P_1$. Among the various Cl_2 bands, the 1 and $2\,^1\Sigma_u^+$ states have been analysed recently (18,19). Note, that the $Cl_2(2\,^1\Pi_u)$ state which dominates in the absorption of pure Cl_2 (18) is nearly absent in the excitation spectra as it is in the excitation spectrum of pure Cl_2 emission (18).

Fig. 3 demonstrates that the monohalide can be produced both under primary excitation of the Ar atom and of the Cl_2 molecule. The branching ratio between $ArCl^*$ and $Cl_2^*(2^3\Pi_g)$ emission is a function of excitation wavelength. As a measure of this ratio we take the ratio of the peak intensities of the excitation spectra.

In Fig. 4a, this is plotted as a function of the vibrational quantum number of $2\,^1\Sigma_u^+$ for three different mixtures. All three curves can be extrapolated to approximately the same onset at $\lambda = 1285 \pm 5$ Å (9.65 eV). Care was taken with the superposition at 1750 Å of the $Cl_2^*(^1\Sigma_u^+)$ fluorescence and the $ArCl^*$ (B-X) emission, especially for the lowest Ar pressure and the 1280 Å $Cl_2\ 2\,^1\Sigma_u^+(v'=0)$ excitation wavelength (18). To within the accuracy of our measurements, for excitation wavelengths below

1200 Å, the ratio is independant of excitation wavelength down to $\sim$ 1100 Å. It depends however on the pressure conditions. The decrease of the branching ratio $I(ArCl)/I(Cl_2\,2^3\Pi_g)$ with increasing pressure (Fig. 4a) probably reflects the collisional relaxation of the initially excited Cl_2 $(2\,^1\Sigma_u^+, v')$ levels towards v'=0 one or to even lower levels of the $1\,^1\Sigma_u^+$ state. Indeed v'=0 of the $2\,^1\Sigma_u^+$ state is close to the energy threshold of $ArCl^*$ formation (σ_f =0) while the production of the $2^3\Pi_g$ state by collisional intersystem crossing is still efficient down to a Cl_2 excitation wavelength of 1470 Å (29).

More insight into the pathways of formation of $ArCl^*$ and population of $Cl_2^*(2^3\Pi_g)$ following initial excitation of $Cl_2^*(2\,^1\Sigma_u^+)$ is obtained by normalizing the individual excitation spectra to the absorbed excitation intensity. This is a rather delicate procedure because the amount of excitation intensity absorbed within that part of the gas cell which is observed by the analysing monochromator is not known well enough for a quantitative analysis. For a qualitative analysis, we assume an optically thin medium, which seems to be justified for 1 torr Cl_2. Then we can normalize to the absorption cross sections of the $2\,^1\Sigma_u^+$ vibrational levels which have been measured recently (18). Fig. 4b shows the results. For $ArCl^*$ fluorescence, we get a monotonic increase up to v'=3 and then a slight decrease. The $Cl_2^*(2^3\Pi_g)$ emission has a pronounced peak at v'=1.

3-2) Formation of $ArCl^*$ and population of Cl_2 ($2^3\Pi_g$) after Cl_2^* excitation

The threshold for $ArCl^*$ formation is explained in Fig. 5 which shows schematically the entrance channel of the reaction of Cl_2^* with Ar. It includes the possibility that an intermediate complex $Cl_2^-Ar^+$ may be involved. The energy of Cl_2 $2^1\Sigma_u^+$,v' and the asymptote $Ar + Cl^+ + Cl^-$ are arranged in a correct scale taking into account the binding energy of $Cl_2(X)$ (D_e = 2.51 eV) (30). The asymptote of the $ArCl^*$ state, $Ar^+(^2P_{3/2}) + Cl^-(^1S_0)$ is calculated from the ionization energy of $Ar^+(IP(^2P_{3/2})$ = 15.76 eV) and electron affinity of Cl^- (3.615 eV) (31). The splitting of the $ArCl^*$ potential curve into the B and the C state is indicated schematically. The C state is positioned above the B state, which follows from our time resolved study (Sec. 4). The potential curve is approximated with the model proposed by Brau and Ewing (32). Within .1 eV, the energy of the minimum, E_m, coincides with $E_{th} - D_e$. Therefore we interprete the measured threshold E_{th} as the energetic threshold of the reaction $Cl_2^* + Ar \rightarrow ArCl^* + Cl$. In other words, E_{th} allows a direct measurement of the energy of the minimum of the lowest $ArCl^*$ state (more precisely speaking : of v'=0 of the $ArCl^*$ (B) state).

Next we discuss the monotonic increase of $ArCl^*$ emission as a function of the vibrational level of the $Cl_2 2^1\Sigma_u^+$ state (Fig. 4b). A few selected excited states of Cl_2 are presented in Fig. 6 (33), which obviously play a role in $ArCl^*$ formation. As is

indicated by the dotted lines, $2^1\Sigma_u^+$ and the double well state $1^1\Sigma_u^+$ result from an avoided crossing of two diabatic states of the same symmetry. In a recent fluorescence study on pure Cl_2 (19) it was shown that the decay of $2^1\Sigma_u^+$ arises partly from predissociation and partly from diabatic crossing of the gap between 2 and $1^1\Sigma_u^+$, followed by radiative decay of $1^1\Sigma_u^+$. The yield of the radiative process in pure Cl_2 (included in Fig. 4b) increases with increasing vibrational quantum number, v', of $2^1\Sigma_u^+$. This increase could be correlated with the Landau-Zener probabilities for the diabatic crossing of the gap (19). The yield of the radiative process (Fig. 4b) shows qualitatively the same dependence on v' as the yield of $ArCl^*$ emission in Ar/Cl_2 mixtures. It thus appears that the precursor for $ArCl^*$ formation is the ionic $1^1\Sigma_u^+$ state though Cl_2 is initially excited in its $2^1\Sigma_u^+$ state.

The reaction $Cl_2^*(1^1\Sigma_u^+) + Rg \rightarrow RgCl^* + Cl$ was recently called a displacement reaction instead of a harpooning reaction since it involves the displacement of the Cl^+ ion of the $Cl_2(1^1\Sigma_u^+$) ionic state by an Rg^+ ion to give the $RgCl^*$ ionic state (34). Note however that it also involves an electron jump from the Rg neutral atom towards Cl^+ in the transition state of the triatomic ($Rg \ldots Cl^+ Cl^-$) collision complex as in a usual $Rg^* + Cl_2 \rightarrow RgCl^* + Cl$ reaction. In (34), this displacement reaction was excluded for $Ar + Cl_2(1^1\Sigma_u^+)$ collisions because the ionization energy of Ar is higher than the ionization energy of the $Cl^+(^1D)$ state in which Cl_2 ($1^1\Sigma_u^+$) dissociates. This argument is correct in the asymptotic limit, but the situation may be different if both the dissociation and internal energies of the molecular species involved in the reaction are properly taken into account to guarantee energy

conservation.

The population of the $2^3\Pi_g$ state of Cl_2 in Ar/Cl_2 mixtures after initial excitation of ungerade states is ascribed to collision induced intersystem crossing. This process clearly takes place, when Cl_2 is excited into the $1^1\Sigma_u^+$ state (19). A direct proof is the huge maximum in the excitation spectrum of Cl_2 2580 Å emission at excitation wavelengths around 1350 Å (Fig. 3).

The peculiar behaviour of the yield of $Cl_2(2^3\Pi_g)$ emission (Fig. 4b) with its peak at v'=1 of $2^1\Sigma_u^+$, however, is explained in the following way. The ab initio calculations of the Cl_2 potential curves (33) predict a crossing of the $3^3\Pi_g$ state with the $2^1\Sigma_u^+$ state near its minimum (Fig. 6). The $3^3\Pi_g$ state is related to the emitting $2^3\Pi_g$ state in a similar way as $2^1\Sigma_u^+$ is to $1^1\Sigma_u^+$. The peak in the yield of $2^3\Pi_g$ emission is obviously due to a maximum in the collision induced intersystem crossing probability and gives strong evidence that $3^3\Pi_g$ crosses $2^1\Sigma_u^+$ near to v'=1 giving rise to large FC overlap integrals. So, our result adds another piece of knowledge to an experimental determination of Cl_2 potential curves and demonstrates once more the quality of the ab initio potentials calculated by Peyerimhoff and Buenker (33).

4 - Time resolved studies

4-1) Introductory remarks

The time evolution of $ArCl^*(B)$ and $Cl_2(1^1\Sigma_u^+)$ emissions under selective Cl_2 excitation was reinvestigated as a function of the partial pressures of Ar and Cl_2. Our goal was to check the radiative lifetimes and quenching rate constants previously measured (14) and to determine the C state energy from the effect of pressure induced B/C mixing in $ArCl^*$. For this later purpose, numerous time profiles of the $ArCl^*$ 1750 Å fluorescence were studied for a great variety of Ar/Cl_2 mixtures and specific Cl_2 excitation energies. In particular the threshold region of $ArCl^*$ B and C state formation was thoroughly examined by exciting Cl_2 in the $2^1\Sigma_u^+$ vibronic progression (18), namely at 1280 (v'=0), 1265 (1), 1250 (2), 1223 (4) and at 1180 Å. In general the pressure of chlorine was in the range 0-10 torr and the argon pressure varied between 5 and 500 torr.

Fig. 7 compares the fluorescence spectra of pure Cl_2 and of two different Ar/Cl_2 mixtures excited at λ_{exc}=1280 Å. A particular difficulty of the ArCl kinetic study, by means of the $Cl_2(2^1\Sigma_u^+) + Ar \rightarrow ArCl^* + Cl$ entrance channel, is that the structured bound-free emission $1^1\Sigma_u^+ \rightarrow X^1\Sigma_g^+$ of Cl_2 is superimposed on the $ArCl^*$ ($B \rightarrow X$) fluorescence at 1750 Å. We thus first studied the kinetics of the Cl_2^* precursor state, in order to safely distinguish in a time signal at 1750 Å what is due to Cl_2^* and what is due to $ArCl^*$.

4-2) Kinetics of the Cl_2^* precursor states

Fig. 7 shows that the $ArCl^*$ signal at 1750 Å is hardly visible with 30 torr of argon while the $Cl_2(2^3\Pi_g \rightarrow 1^3\Pi_u)$ fluorescence at 2580 Å is intense. At 200 torr of argon, the Cl_2 $(1^1\Sigma_u^+)$ fluorescence is strongly quenched and ArCl (B-X) emission at 1750 Å is clearly seen.

For the lifetimes and quenching rates determination, best observation wavelengths were determined by taking the specific Cl_2 fluorescence spectrum for each excitation energy used in this study. These spectra show beautiful bound-bound and bound-free features. These features were observed before, but only in part, due to the SiO_2 window detector used in our previous investigation (18). The observation wavelength is now choosen outside the emission spectrum of $ArCl^*$ (B-X as well C-A transitions) and as close as possible to the excitation wavelength. This eliminates the effect of vibrational relaxation which results, at longer analysis wavelengths, in lower values of the quenching rate constants.

Fig. 8 shows some of our results and Table I reports the measured values of the various rate constants and lifetimes. Quenching of Cl_2^* by Cl_2 is very efficient and results in V-V transfer or excitation of other Cl_2^* states which may dissociate or not. Good agreement is found with the recent work of Zuev et al. (35) based on luminescence absolute quantum efficiencies measurements.

The radiative lifetimes we determined for different levels of the $1^1\Sigma_u^+$ or $2^1\Sigma_u^+$ states are similarly short, ≈3 ns. That of

the state reached at λ_{exc}=1180 Å is even shorter.

Ar collisions, as was shown in the first part of this paper, lead to intersystem crossing to the $2^3\Pi_g$ state and/or to $ArCl^*$ formation, depending on the initial Cl_2^* excitation energy. We find no drastic change in the rate constant k(Ar) with the excitation energy, i.e whether the formation of $ArCl^*$ is possible or not. Note that k(Ar) is the total deexcitation rate constant of the primary Cl_2^* excited state, i.e., the sum of the individual formation rate constants of all the products.

Before discussing the $ArCl^*$ kinetics, we can point out for accuracy that the time profiles of the Cl_2^* emissions always contain an additional slow component of low intensity. Its assignment will not be discussed in this paper. It is only worthwhile to say that, for P(Ar) over 10-15 torr, both components of the Cl_2^* emission decay faster than any decay from $ArCl^*$. Moreover, due to the reactive collisions with Ar, the Cl_2^* signal is rapidly quenched and does not hinder too much the evaluation of the $ArCl^*$ signal.

4-3) Kinetics near threshold excitation. Determination of the radiative lifetime and quenching rate constants of $ArCl^*(B)$

In the first part of this paper, we have shown that an initial excitation of the Ar/Cl_2 system at 1280 Å allows $ArCl^*$ to be obtained at the bottom of the B well, very near its formation threshold which was estimated at 1285 Å.

Fig. 9a shows some examples of time profiles obtained for λ_{exc}=1280 Å. At the top of the figure, one curve (*) corresponds to Cl_2^* emission with an analysis wavelength of 1290 Å. All the

other curves are obtained at λ_{an}=1750 Å with different Ar/Cl_2 mixtures. The chlorine pressure is fixed to 0.8 torr.

Whatever the Ar pressure, the time profile of the 1750 Å emission always has a prompt onset. For low P(Ar), this is due to the primary Cl_2^* fluorescence which is identified, in the 1750 Å time profile, by comparison with the pure Cl_2^* signal for the same argon pressure. At higher argon pressures, the primary Cl_2^* signal is quenched (see Fig. 7) but the formation process of the $ArCl^*$ (B,v'=0) emitting level is very fast, due to the short radiative lifetime of the Cl_2^* precursor state and to the high rate constant of its reaction with Ar.

Fig. 10 presents the decay rates we have evaluated on the late exponential part of the $ArCl^*$ decay (Fig. 9a) and the corresponding fitted values obtained with the two-exponential Stricker program (24). This comparison shows the general good agreement between the two determinations. One sees that our evaluations give a weaker scatter together with good approximate values of the decay rates.

For high P(Ar), a weak and fast primary peak persists in the early times of the 1750 Å signal decay (Fig. 9a). It probably arises from the Cl_2^* fluorescence. Other low v'>0 $ArCl^*$(B) levels might be initially formed at the 1280 Å entrance energy and also emit at the 1750 Å analysis wavelength. These levels would obviously decay faster than the v'=0 level due to their additional vibrational relaxation loss term and eventually to some energy transfer term with the C state. At high P(Ar) the early decay rate is clearly different from that of the (B,v'=0) level whose P(Ar) dependence has a simple parabolic shape. At low P(Ar), the small

deviation of the measured decay rates with respect to the parabola is ascribed to the contribution of the superimposed signal whose decay rate can not be distinguish from that of the (v'=0) level between 5 and around 70 torr.

The decay rates of the $ArCl^*$ (B,v'=0) level thus obeys the quadratic expression (I)

$$1/\tau = 1/\tau_o + k_1(Ar)[Ar] + k_2(Ar)[Ar]^2 \qquad (I)$$

in which $1/\tau_o$ is the intercept for P(Ar)=0 at the particular Cl_2 pressure. The two and three-body quenching rate constants with argon as well as the radiative lifetime, deduced from experiments where $P(Cl_2)$ was varied (see below) are given in Table II.

Fig. 11 presents our results of the quenching of $ArCl^*$ (B,v'=0) by Cl_2 collisions. P(Ar) is fixed (49 torr) and $P(Cl_2)$ varied between 0 and 10 torr. The slope gives the value of the rate constant (Table II). Note that similar determinations of $k(Cl_2)$ where done for other excitation energies and various argon pressures. No systematic variation of the rate constant was obtained within the limits of the experimental error. The different intercepts observed (Fig. 11) for the same argon pressure but different excitation energies are discussed in part 4-4).

We thus conclude, from the pure quadratic expression (I) that the $ArCl^*$(B,v'=0) level is a pure decaying state. This is a different situation from the $XeCl^*$ and $KrCl^*$ systems (21) where the (B,v'=0) level is collisionally mixed with the C state. That means that the $ArCl^*$(C) state is not initially formed by the 1280 Å excitation and that the (B,v'=0) level can not transfer energy to it by collision. The C state is thus located at a somewhat higher

energy than B.

4-4) Kinetics of $ArCl^*$ under higher excitation energies

Fig. 9b and 9c present some of the time profiles obtained at λ_{an}=1750 Å for different argon pressures of the Ar/Cl_2 mixture excited at 1250 and 1180 Å. For λ_{exc}=1250 Å (Fig. 9b), the first curve is a pure Cl_2^* decay. Low P(Ar) curves show the early Cl_2^* signal before the decay due to $ArCl^*$. Some deviation from a pure exponential $ArCl^*$ decay is nevertheless suspected. For high P(Ar), the chlorine emission is quenched and a rise component is visible ; moreover a low intensity additional slow decay component appears. For λ_{exc}=1180 Å (Fig. 9c), the rise and long components are more important and can be evaluated.

The two other excitation wavelengths used (1265 and 1223 Å) give time profiles somewhat similar and are not shown. For λ_{exc}=1265 Å the rise component begins to be visible at high P(Ar), but not yet the slow decay.

Because of the Cl_2^* fluorescence, nothing can be said about the rise component of the $ArCl^*$ signal at low P(Ar). However at high P(Ar), the clear rise observed must at least contain information on the vibrational relaxation from the firstly obtained $ArCl^*$ high levels to the v'=0 one observed at 1750 Å.

Computer fits of the high P(Ar) time profiles with a three-exponential program correctly agree with hand evaluations of the fast and slow decay components. However the computer procedure is long and gives sometimes unreliable results. We thus prefered our direct measurements of the slopes of the decay curves in the

semilogarithmic scale, knowing that they only give approximate but reliable values of true decay rates.

Fig. 12 gives such determination of our "decay rates" and the mean P(Ar) dependence for the time profiles obtained at 1250 and 1180 Å. The 1280 Å parabola is also shown for comparison as well as rough estimations of the rates of the rise and slow decay component for λ_{exc}=1180 Å.

Compared to experiments at λ_{exc}=1280 Å, higher excitation energies lead to large deviations from the simple parabolic shape at low P(Ar) (Fig. 12). The difference, which is already important between 1280 and 1265 Å excitations, decreases with the higher energies. A systematic trend seems to exist in the "decay rates" obtained at the same argon pressure with the five excitation energies used in this study (21).

The inflexions observed on the $1/\tau = f(P(Ar))$ curves were already found in the $XeCl^*$ and $KrCl^*$ systems and satisfactorily explained by the two level collisional mixing of the B and C states (21). In those cases, in spite of the fact that the RgCl systems are excited in high vibronic levels, the vibrational relaxation to the v'=0 level is fast and does not interfere with the λ^- component of the collisionally B/C mixing and decay process of the B state (21).

In the $ArCl^*$ system, the differences observed between 1280 Å and higher excitation energies show 1) the critical importance of the excitation wavelength on the C state initial population, i.e. the C state must be significantly above the B state and 2) that vibrational relaxation in the $ArCl^*$ case is not fast enough, since we see an effect of the excitation energy on the apparent "decay

rate" of the $ArCl^*(B,v=0)$ level.

An attempt for a purely empirical determination of the threshold of the C state formation is presented on Fig. 13. For that purpose, the $ArCl^*$ decay rates deduced from the curves shown on Fig. 12 are plotted for specific argon pressures as a function of the different Cl_2 excitation wavelengths. For a given P(Ar), $1/\tau$ values are nearly the same for the three higher energies, but are very different for the 1265 and 1280 Å excitations. The lines thus defined cross at a λ_c value which linearly decreases with increasing argon pressure, as it is shown in the lower part of the figure. We believe that the wavelength of the P(Ar)=0 extrapolation ($\sim$ 1260 Å), for which no collisional vibrational relaxation effect can occur, is a good estimation of the C state excitation threshold in the Ar/Cl_2 system.

The 1285 and 1260 Å values we have thus determined experimentally for the excitation thresholds of $ArCl^*$ B and C states in the Ar/Cl_2 system correspond to a $\Delta E(B-C)$ energy difference of $\sim$ 1600 cm^{-1}. This is much higher than in the $XeCl^*$ and $KrCl^*$ systems where the simple two-level B/C mixing model was applied satisfactorily (21). With such a high $\Delta E(B-C)$ value, the two level model predicts a pseudo crossing of the λ^+ and λ^- P(Ar) dependences (21), which is not observed in the case of $ArCl^*$ (Fig. 12). Therefore comparing $\Delta E(B-C)$ with a vibronic quantum and considering the effect of the vibrational relaxation in the $ArCl^*$ system led us to test the following theoretical two-ladder B/C mixing and relaxation model.

4-5) The ArCl two-ladder multilevel mixing and relaxation model

The basic assumptions of the simplified $ArCl^*$ two-ladder multilevel mixing and relaxation model are the following :

1) We assume an harmonic potential for the B and C states of $ArCl^*$ with ω_e=281 cm^{-1} taken from the KCl (X) ground state (36).
2) Overlap of levels v'(B)=6 with v'(C)=0 ; v'(B)=7 with v'(C)=1 etc ..., up to v'(B)=10 with v'(C)=4. The mixing rate constant for these coresponding levels are set so that kBC=k1=kCB. We thus suppose an activation energy between B and C of $\sim$ 1700 cm^{-1}.
3) It is assumed that the rate constant for the downwards mixing transitions between B and C are identical for an equal energy gap ΔE. For instance, from B(v'=7) to C(v'=0) kBC70=kCB05 ; kBC80=kCB04 etc ... An energy gap law is assumed to be valid for these downwards transitions, for example $kBC70=k1\ \exp(-\Delta E/kT.)$ In the case of the upwards transitions, identical rate constants for equal energy gaps were also used, for example kBC50=kCB07, kBC40=kCB08, etc ... Upwards and downwards transitions have been coupled by the principle of detailed balancing (37).
4) According to the results of a first order perturbation approximation FOPA (38) theory, the vibrational relaxation has been described by :

$kRB(v+1,v)=(v+1)kRB(1,0)$ and

$kRB(0,1)=kRB(1,0)\ \exp(-\Delta E/kT)$

for both the B and C vibronic manifolds with kRB(1,0)=kRC(1,0).

5) The quenching of the B and C states in two or three-body collisions was assumed to be independant of the vibrational quantum number and to be identical for both the B and C states.

6) The radiative lifetime of the B state (τ_B=5.2 ns), derived from our results, assumed independent on v'B) ; a C state lifetime of τ_C=48 ns (independent on v'C) and a radiative lifetime of the $Cl_2^*(2^1\Sigma_u^+)$ state of 3.2 ns (independent on v'$Cl_2^*(2^1\Sigma_u^+)$) have been used throughout all our calculations.

7) It was assumed that, within the bandpass of our secondary monochromator, only the B to X transition from v'=0 was detected. For three distinct cases of excitation energy of Cl_2^*, the time profiles of the $ArCl^*$(B,v'=0) fluorescence were calculated for a variety of Ar pressures. The two and three-body quenching rates by Ar and Cl_2 were taken from the present results (Table II). It was assumed that the harpooning reaction (1) has a rate constant of 9.0 x 10^{-10} cm^3s^{-1} and unit quantum efficiency

$$Cl_2(2^1\Sigma_u^+, v') + Ar \longrightarrow ArCl^* + Cl \qquad (1)$$

so that the quenching rate k of Cl_2 states by Ar collisions measured in this study leads only to $ArCl^*$ pumping. The calculations were carried out using the computer program FAKSIMILE to solve the very complex set of differential equations. In the first case, a δ-like population of $Cl_2(2^1\Sigma_u^+, v'=0)$ is supposed to lead only to the pumping of $ArCl^*$(B,v'=0) level. In the second case, from v'=2 of Cl_2^*, one pumps v'B=6 and v'C=0 with the same rate. In the last case, the excitation of v'B=10 and v'C=4 was supposed from $Cl_2^*(2^1\Sigma_u^+, v'=3)$ excitation, also with identical rates. The population of the lower B and C vibronic levels

from the primarily excited Cl_2^* was neglected. All calculations were carried out over 20 orders of magnitude of the $ArCl^*$(B,v'=0)→ ArCl(X) intensity. This intensity, the decay rate

$$K = \frac{\log I(t+\Delta t) - \log I(t)}{\Delta t}$$

and the population for each B and C vibronic levels were computed for at least 400 steps in time.

Some of the calculated time profiles of the $ArCl^*$(B,v'=0)→ ArCl(X) emission are shown on Fig. 14. They are in good qualitative agreement with the observed fluorescence signals of Fig. 9. Except for the first case of excitation, all time profiles, when plotted in a semilog scale, show a slight curvature in the early decay portions of the fluorescence signal. In order to compare the computed decay rates with the observed hand-evaluated values, an average of K at Imax/10 and Imax/1000 was choosen.

A comparison of the computed Ar pressure dependences of K for the three cases of excitation, with our experimental results, are shown in Fig. 15. A fair agreement between computed and experimental values of K was obtained by using kBC=k1=1.1 x 10^{-10} cm3s-1 for the Ar pressure induced mixing of B and C states at energy resonance and a value of kRB(1,0)=2.5 x 10^{-11} cm^3s^{-1} for the relaxation in the B and C manifolds. The general behaviour of K, at low Ar pressures, at which pronounced differences in the pressure dependence of the decay rates were experimentally found for different excitations energies (Fig. 12), is well described by the model.

At high P(Ar), where the three curves appear to be parallel

and shifted in K, the relaxation to $ArCl^*(B,v'=0)$ seems to be the rate controlling step. Agreement with the experimental results at high Ar pressure was only achievable under the assumption that the V-T relaxation is slow compared to the mixing of B and C by collisions.

Due to the numerous assumptions made and to the time consuming nature of these calculations, we did not intend to extract from a better agreement between model and experiment the absolute values of some missing rate constants. However, the model is interesting and useful and perfectly confirms how and why it is difficult to study experimentally the physical $ArCl^*$ system.

Moreover we have to note that the present model can not explain the additional late decay component which appears for high P and high excitation energies. This point is further discussed below.

4-6) Comparison with other works

Owing to several experimental improvements, mainly in spectral and time resolution, and to a better general knowledge and a much more precise description of the physical system, lifetimes and rate constants presented in this paper take precedence over those reported in our earlier work (14).

Thus our firstly reported $ArCl^*$ high quenching rate $k(Ar)[Ar]$ is now seen as the sum of a two-body $k1(Ar)[Ar]$ and a three-body $k2(Ar)[Ar]^2$ term (Table II) which have the same order of magnitude as the corresponding terms of krypton and xenon

chlorides (21,39,40). Our three-body rate constant $k2(Ar)=1.4\times10^{-30}$ cm^3s^{-1} is much higher than that recently reported by Liegel et al (7) in an e- beam pulse radiolysis study of Ar/RCl mixtures. However we believe that our value is more reliable if we compare several respective experimental parameters of both studies, in particular : selectivity of the primary formation process and of the excitation and observation wavelengths, time resolution in excitation and detection, direct or relative way of data determination, etc ...

Generally measurement of the radiative lifetime of a $RgCl^*(B)$ state is not an obvious task. As a matter of fact, a survey of the literature clearly shows that, depending on experimental conditions (low or high pressure experiments, variable entrance energy in the system), different values of τ_{rad} have been obtained. For $ArCl^*$, very few determinations have been reported. In low P experiments, Gundel et al. report values of the order of 100 ns (9) while high P studies, or experiments in which $RgCl^*$ is formed in the bottom of the B potential well, yield much lower values of 10-20 ns. These discrepancies are due to two main reasons : i) a strong dependence of the radiative lifetime with the vibrational energy (41), hence an important effect of the entrance energy and of the vibrational relaxation process ; ii) an efficient collisional B/C mixing of the low levels of B and C states which results in an effective lifetime longer than the radiative one of the $ArCl^*(B,v'=0)$ state of 5.2 ns.

The energies we determine for $ArCl^*$ B and C states agree with the work of Gundel et al. (9). Indeed these authors, by the reaction of Ar $^3P_{2,0}$ metastables with HCl, obtained $ArCl^*(B-X)$

emission from the lowest levels of the B state without any C-A fluorescence. If ArCl (B) is formed from $Ar\ ^3P_2$ metastable, this means that $Ar\ ^3P_0$ can't excite $ArCl^*$(C). From the knowledge of the respective dissociation energies of HCl and Cl_2, we deduce an estimation of the energy threshold of B and C states in the Ar/Cl_2 system. The B state threshold would then occur at λ_{exc} slightly above 1292 Å and that of the C state at λ_{exc} slightly below 1268 Å, in very good agreement with our findings.

The reaction $Ar^* + Cl_2$ was also studied by Golde and Poletti who have found that $Ar\ ^3P_2$ yields mainly the B state while $Ar\ ^3P_0$ forms preferentially the D state as shown by their $ArCl^*$(D-X) emission spectrum in the 1500-1800 Å region (10). The threshold excitation energy of the D state can be estimated to be λ_{exc} =1265 Å in the Ar/Cl_2 system, that means just in the region where we estimated the C state energy.

In the particular case of $ArCl^*$, an additional difficulty thus occurs, with the eventual participation of the D state to the B/C mixing process. The D → B collisional state transfer was already suspected in similar recent studies of XeF^*(42), KrF^*(43) and $ArCl^*$ itself (44). It might be useful to consider a B/C/D mixing model for a complete description of the $ArCl^*$ system. In any case, this discussion shows the crucial need for clean experiments and careful studies for any significant investigation of this surprisingly complicated ArCl system.

No doubt that theoretical developments of the work would be useful in the future, in particular the study of these multisurface reactive collision processes, with spin-orbit coupling, by means of symmetry correlation diagrams in linear or

bent configuration of the (Ar,Cl_2^*) collision complex.

5 - Summary

By using the experimental station for fluorescence spectroscopy of the Synchrotron Radiation Laboratory HASYLAB / DESY Hamburg, stationary and time-resolved fluorescence spectroscopy of the Cl_2^* $(1^1\Sigma_u^+)(2\Sigma_u^+)$ and $ArCl^*$(B) emissions have been studied in much more detail than before in the Ar/Cl_2 system.

The entrance channel from excited vibronic states of Cl_2 (Cl_2^* + Ar → products) was mainly exploited. Depending on the initial excitation energy of Cl_2, either $Cl_2^*(2^3\Pi_g)$ state or both $Cl_2^*(2^3\Pi_g)$ and $ArCl^*$(B) (and (C)) states are populated. Formation of $2^3\Pi_g$ is discussed in terms of collisional inter-system crossing and supports the calculated potential curves from Peyerimhoff et al.(33). Formation of ArCl(B) occurs at the threshold by a mechanism which can be considered to be of the harpoon type.

A detailed time resolved study of the $ArCl^*$ fluorescence is presented. In the Ar/Cl_2 system, special care must be taken for the possible overlap of the $Cl_2^*(1^1\Sigma_u^+ \rightarrow X)$ emission with the $ArCl^*$ (B → X) signal. Much better values of the radiative lifetime and quenching rate constants by Ar and Cl_2 of the $ArCl^*$(B) state have been determined. The C state energy has been experimentally estimated, and the collisional mixing between B and C states is discussed in terms of a two-ladder multilevel relaxation and mixing theoretical model.

The results are compared with the literature data. Finally a last question of this particulary delicate $ArCl^*$ study is the

eventual participation of the D state in the population and decay processes involved.

Acknowledgments

The support of our work by the crew of HASYLAB (Hamburg) is gratefully acknowledged. The authors are indebted to those who have constructed the high intensity beam line and the Superlumi station, mainly Prof. N. Schwentner, Dr H. Wilcke, Dr P. Gürtler and Dr. E. Roick. The work was sponsored by the Bundes Ministerium für Forschung und Technologie (BMFT).

References

1 - M. KRAUSS and F.H. MIES
Excimer Lasers ; Topics in Applied Physics. Vol. 30, pp 5-46
Berlin, Heidelberg, New-York : Springer-Verlag (1979)

2 - P.J. HAY, T.H. DUNNING
J. Chem. Phys. 69, 2209 (1978)

3 - T.H. DUNNING, P.J. HAY
J. Chem. Phys. 69, 134 (1978)

4 - CH. A. BRAU
Excimer Lasers ; Topics in Applied Physics Vol. 30, pp 87-133
Berlin, Heidelberg, New-York : Springer-Verlag (1979)

5 - T.H. JOHNSON, A.M. HUNTER
J. Appl. Phys. 51, 2406 (1980)

6 - R. SAUERBREY, W. WALTER, F.K. TITTEL, W.L. WILSON
J. Chem. Phys. 78, 735 (1983)

7 - J. LIEGEL, H. SPIEGEL, R. SAUERBREY and H. LANGHOFF
J. Chem. Phys. 79, 247 (1983)

8 - J.E. VELAZCO, J.H. KOLTS, D.W. SETSER
J. Chem. Phys. 65, 3468 (1976)

9 - L.A. GUNDEL, D.W. SETSER, M.A.A. CLYNE, J.A. COXON, W. NIP
J. Chem. Phys. 64, 4390 (1976)

10 - M.F. GOLDE, R.A. POLETTI
Chem. Phys. Lett 80, 23 (1981)

11 - K. TAMAGAKE, J.H. KOLTS, D.W. SETSER
J. Chem. Phys. 71, 1264 (1979)

12 - G. INOUE, J.K. KU, D.W. SETSER
J. Chem. Phys. 80, 6006 (1984)

13 - D.W. SETSER, J. KU
Photophysics and photochemistry above 6 eV, pp 621-637,
Amsterdam : Elsevier 1985

14 - M.C. CASTEX, J. LE CALVÉ, D. HAAKS, B. JORDAN, G. ZIMMERER
Chem. Phys. Lett 70, 106 (1980)

15 - J. LE CALVÉ, M.C. CASTEX, D. HAAKS, B. JORDAN, G. ZIMMERER
Il Nuovo Cimento 63 B, 265 (1981)

16 - B. JORDAN
Thesis, University of Hamburg (1983)

17 - G. ZIMMERER
Photophysics and photochemistry above 6 eV, pp 357-374
Amsterdam : Elsevier 1985

18 - T. MÖLLER, B. JORDAN, P. GURTLER, G. ZIMMERER, D. HAAKS, J. LE CALVE, MC. CASTEX
Chem. Phys. 76, 295 (1983)

19 - T. MÖLLER
Diploma work, University of Hamburg (1982) and Int. Report DESY F41 - HASYLAB 82-07 (1982)

20 - A.E. DOUGLAS
Can. J. Phys. 59, 835 (1981)

21 - J. LE CALVÉ, M.C. CASTEX, B. JORDAN, G. ZIMMERER, T. MÖLLER, D. HAAKS
Photophysics and photochemistry above 6 eV, pp 639-651
Amsterdam : Elsevier 1985

22 - V. HAHN, N. SCHWENTNER, G. ZIMMERER
Nucl. Instr. and Meth. 152, 261 (1978)

23 - I.H. MUNRO, N. SCHWENTNER
Nucl. Instr. and Meth. 208, 819 (1983)

24 - G. STRIKER
Private communication

25 - H. WILCKE, W. BOHMER, R. HAENSEL, N. SCHWENTNER
Nucl. Instr. and Meth. 208, 59 (1983)

26 - P. GÜRTLER, E. ROICK, G. ZIMMERER, M. POUEY
Nucl. Instr. and Meth. 208, 835 (1983)

27 - M. Mc CUSKER
Excimer Lasers ; Topics in Applied Physics. vol. 30, pp 47-86
Berlin, Heidelberg, New-York : Springer-Verlag 1979

28 - M. DIEGELMANN, K. HOHLA, F. REBENTROST, K.L. KOMPA
J. Chem. Phys. 76, 1233 (1982)

29 - Y.C. YU
Ph. D. Thesis, Kansas State University (1984)

30 - K.P. HUBER, G. HERZBERG
Molecular Spectra and Molecular Structure ; New-York, Toronto van Nostrand Reinhold Company (1979)

31 - H.M. ROSENSTOCK, K. DRAXL, B.W. STEINER, J.T. HERRON
J. Phys. and Chem. Ref. Data 6, Sup. 1 (1977) Energetics of gaseous ions, N.B.S. publication

32 - C.A. BRAU and J.J. EWING
J. Chem. Phys. 63, 4640 (1975)

33 - S.D. PEYERIMHOFF, R.J. BUENKER
Chem. Phys. 57, 279 (1981)

34 - M.W. WILSON, M. ROTHSCHILD, C.K. RHODES
J. Chem. Phys. 78, 3779 (1983)

35 - V.S. ZUEV, A.V. KANAEV, L.D. MIKHEEV
Sov. J. Quantum. Electron. 14, 242 (1984)

36 - S.A. RICE, W. KLEMPERER
J. Chem. Phys. 27, 573 (1957)

37 - I.W.M. SMITH
Kinetics and dynamics of elementary gas reactions,
Butterworth Monographs in Chemistry (1981)

38 - D. RAPP, T. KASSAL
Chem. Rev. 69, 61 (1969)

39 - D.C. LORENTS
Lasers'84 Conference and private communication

40 - M.G. DURRETT
Master thesis, University of Houston (1982)

41 - T.D. DREILING, D.W. SETSER
J. Chem. Phys. 75, 4360 (1981)

42 - N.K. BIBINOV, I.P. VINOGRADOV
Sov. J. Quantum. Electron. 13, 1286 (1983)

43 - H. HELM, L.E. JUSINSKI, D.C. LORENTS, D.L. HUESTIS
J. Chem. Phys. 80, 1796 (1984)

44 - J. LIEGEL
Thesis, University of Würzburg (1984)

FIGURE CAPTIONS

Fig. 1 Fluorescence spectrum of 275 torr Ar doped with .3% Cl_2. The gas mixture was excited with the zeroth order radiation of the primary monochromator. The main decay channels are characterized.

Fig. 2 Fluorescence spectra of 275 torr Ar doped with .3% Cl_2 under selective excitation of either Cl_2 (upper curve) or Ar.

Fig. 3 Excitation spectra of $Cl_2^*(2^3\Pi_g)$ emission and of the $ArCl^*$ $B \rightarrow X$ fluorescence in 275 torr Ar doped with .3% Cl_2. The main excitation channels are characterized. The assignments of the Cl_2^* excitations are taken from Ref. (18).

Fig. 4 a) Branching ratio between $ArCl^*$ and Cl_2^* emission as a function of the vibrational quantum number of the primarily excited $Cl_2^*(2^1\Sigma_u^+)$ state. The pressure conditions given are also valid for b).

b) Fluorescence yields of $ArCl^*$ emission (open circles) and of Cl_2^* emission (crosses) as a function of the vibrational quantum number of the primarily excited $Cl_2^*(2^1\Sigma_u^+)$ state.
The triangles display the fluorescence yield of pure Cl_2 (mainly $Cl_2(1^1\Sigma_u^+)$ emission) (19).

Fig. 5 Schematic pathway of $ArCl^*$ formation in collisions of selectively excited Cl_2^* with Ar. The coordinate in the entrance channel is the Cl_2^* - Ar distance. The coordinate of the exit channel is the internuclear distance of ArCl. The arrow on the energy axis represents the minimum of $ArCl^*$ given by Brau and Ewing (32). The second arrow represents the measured threshold of the reaction.

Fig. 6 Potential curves of the Cl_2 molecule (not complete). In the lower part, experimental potential curves are given ($X\,^1\Sigma_g^+$, $1\,^3\Pi_u$ and $1\,^1\Pi_u$)(30). All other potential curves are results of ab initio calculations (33).

Fig. 7 Fluorescence spectra of a) pure chlorine (1 torr) ; b) Cl_2(1 torr) + Ar (30 torr) ; c) Cl_2(1 torr) + Ar (200 torr). The pure Cl_2 spectrum corresponds to $2\,^1\Sigma_u^+$ and $1\,^1\Sigma_u^+ \rightarrow X\,^1\Sigma_g^+$ transitions. Addition of Ar results in the $2\,^3\Pi_g \rightarrow {}^3\Pi_u$ emission at 2580 Å and in $ArCl^*$(B-X) fluorescence at 1750 Å.

Fig. 8 Determination of the Ar or Cl_2 quenching rate constants and radiative lifetimes of different Cl_2^* vibronic states. The lower part of the figure concerns pure Cl_2, the upper part Cl_2^* + Ar mixtures where P(Ar) only is varied. Excitation and analysis wavelengths are indicated.

Fig. 9 Time profiles of the 1750 Å fluorescence signal in Ar + Cl_2 mixtures for two primary excitations of the Cl_2^* $(2\,^1\Sigma_u^+)$state a) 1280 Å (v'=0) ; b) 1250 Å (v'=2) and c) for Cl_2^* excitation at 1180 Å. $P(Cl_2)$ is always 0.8 torr. P(Ar) (torr) is given in each case.

Fig. 10 P(Ar) dependence of the $ArCl^*$(B-X) 1750 Å decay frequency for λ_{exc}=1280 Å corresponding to the Cl_2 $(2\,^1\Sigma_u^+, v'=0)$ state : (•) experimental, (+) fitted values. The parabolic curve is given by equation I (see text). The steep line corresponds to the $ArCl^*$ formation rate (see Fig. 8).

Fig. 11 Determination of the quenching rate constant of $ArCl^*$(B) by Cl_2. The value 5.2 ns for the radiative lifetime of B(v'=0) results from both Fig. 10 and 11 data at λ_{exc} = 1280 Å.

Fig. 12 P(Ar) dependence of the ArCl 1750 Å decay frequency for three excitation wavelengths. Best mean curves through the experimental points are shown. The lines a and b corresponds to the rate of the rise and of the last decay component for λ_{exc}=1180 Å (see fig. 9c).

Fig. 13 Estimation of the $ArCl^*$(C) state formation energy threshold in the Ar/Cl_2 system (see text).

Fig. 14 Computed time profiles of the $ArCl^*$(B,v'=0) emission for the three cases of primary excitation of Cl_2 $(2\,^1\Sigma_u^+)$ v'=0, 2 and 3 (see text). P(Ar) is a) 10 ; b) 100 ; c) 500 torr.

Fig. 15 P(Ar) dependence of the computed decay frequency K of $ArCl^*$ (B,v'=0) emitting level with the two ladder multilevel model used. The three curves correspond to
case a) excitation of B(v'=0)
case b) excitation of B(v'=6) and C(v'=0)
case c) excitation of B(v'=10) and C(v'=4)
For comparison, the measured decay rates for λ_{exc}=1280(•) and 1250 Å (0) are repeated.

Table I - Radiative lifetimes τ and quenching rate constants ($k(Cl_2)$, $k(Ar)$) of various Cl_2^* excited states.

λexc / λan *	1350/1403	1280/1290	1250/1270	1180/1205
	$1^1\Sigma_u^+(v' \sim 40)$	$2^1\Sigma_u^+(v'=0)$	$2^1\Sigma_u^+(v'=2)$	see text
τ (ns)	2.6	2.85		1.4
$k(Cl_2)$ ($cm^3 s^{-1}$)	1.9×10^{-9}	2.7×10^{-9}		2.2×10^{-9}
$k(Ar)$ ($cm^3 s^{-1}$)	9×10^{-10}	9.7×10^{-10}	10.4×10^{-10}	

* the wavelengths (Å) of excitation (λexc) and fluorescence analysis (λan) are specified, with the assignment of the corresponding Cl_2^* excited state.

Table II - ArCl parameters determined in this work

- Spectroscopic parameters (threshold excitation wavelength in the Ar/Cl_2 system)

  B state : 1285 ± 5 Å

  C state : ~ 1260 Å

- Kinetic parameters for $ArCl^*(B,v'=0)$

  Radiative lifetime : τ = 5.2 ns

  Quenching by Cl_2 : $k(Cl_2) = 7 \pm 0.5 \times 10^{-10}$ $cm^3 s^{-1}$

  Two-body quenching by Ar : $k_1(Ar) = 0.4 \times 10^{-11}$ $cm^3 s^{-1}$

  Three-body quenching by Ar : $k_2(Ar) = 1.4 \times 10^{-30}$ $cm^6 s^{-1}$

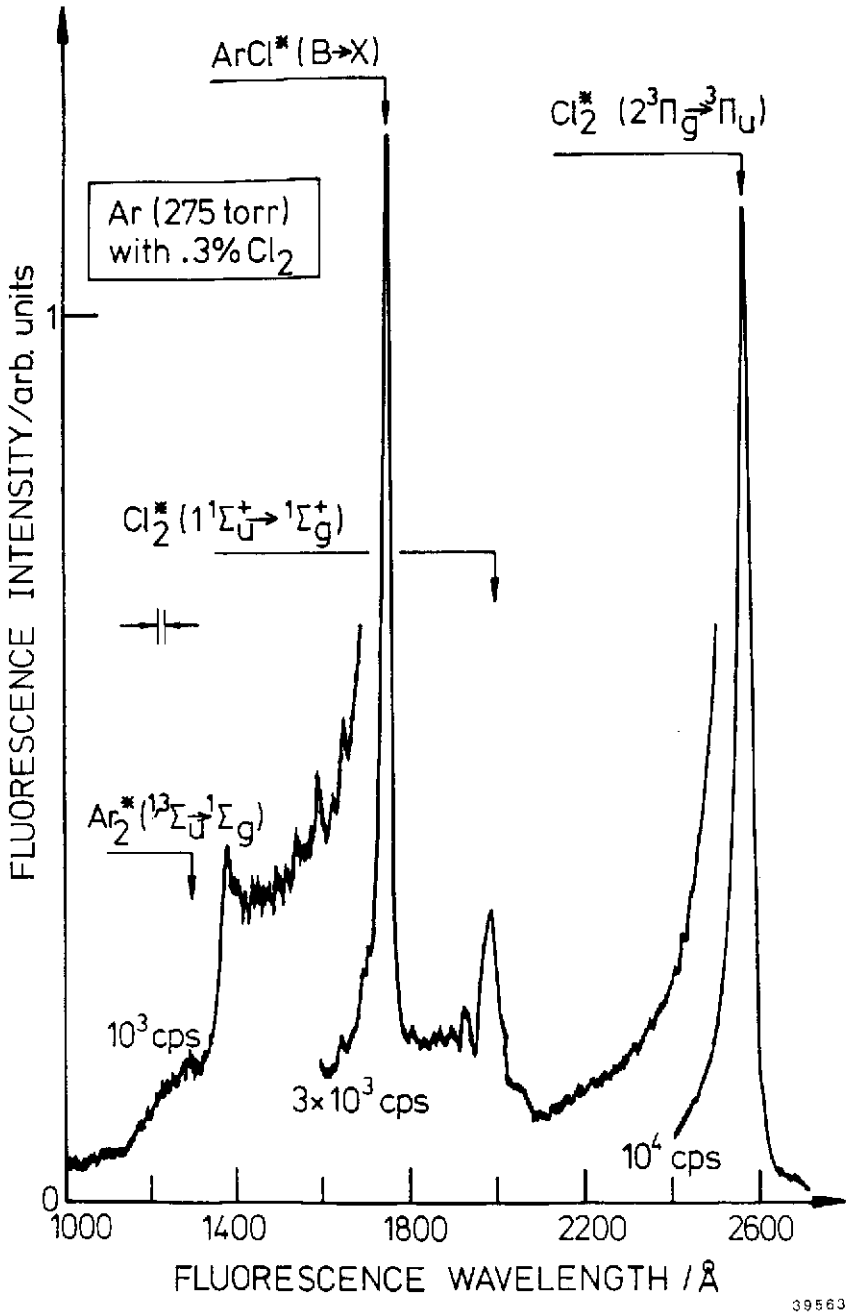
ArCl* (B→X)
Cl2* (2³Πg→³Πu)
Ar (275 torr)
with .3% Cl2
Cl2* (1¹Σu+→¹Σg+)
Ar2* (1,3Σu→¹Σg)
10³ cps
3×10³ cps
10⁴ cps
FLUORESCENCE INTENSITY/arb. units
1
0
1000
1400
1800
2200
2600
FLUORESCENCE WAVELENGTH / Å
39563

Fig. 1

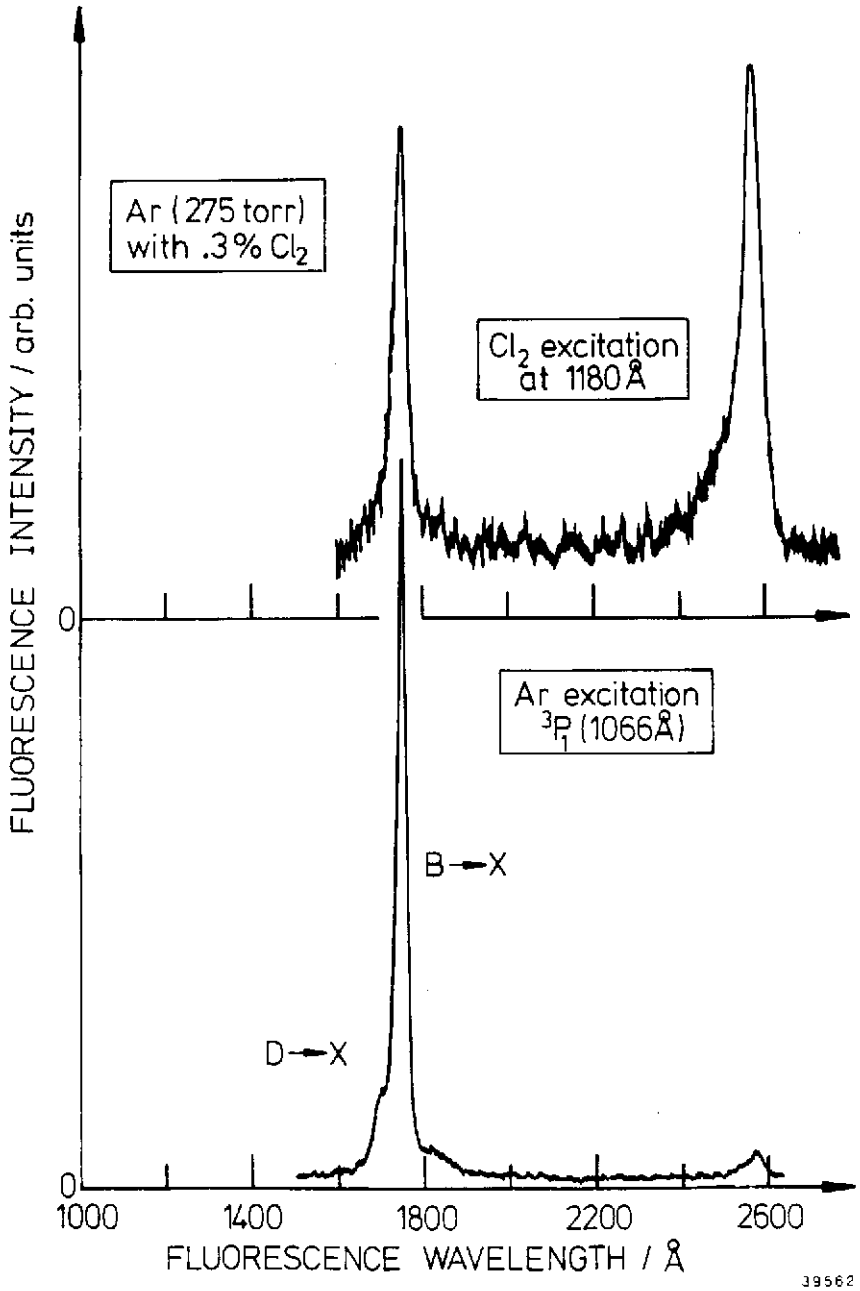
Ar (275 torr)
with .3% Cl2
Cl2 excitation
at 1180 Å
Ar excitation
³P1 (1066Å)
B→X
D→X
FLUORESCENCE INTENSITY / arb. units
0
0
1000
1400
1800
2200
2600
FLUORESCENCE WAVELENGTH / Å
39562

Fig. 2

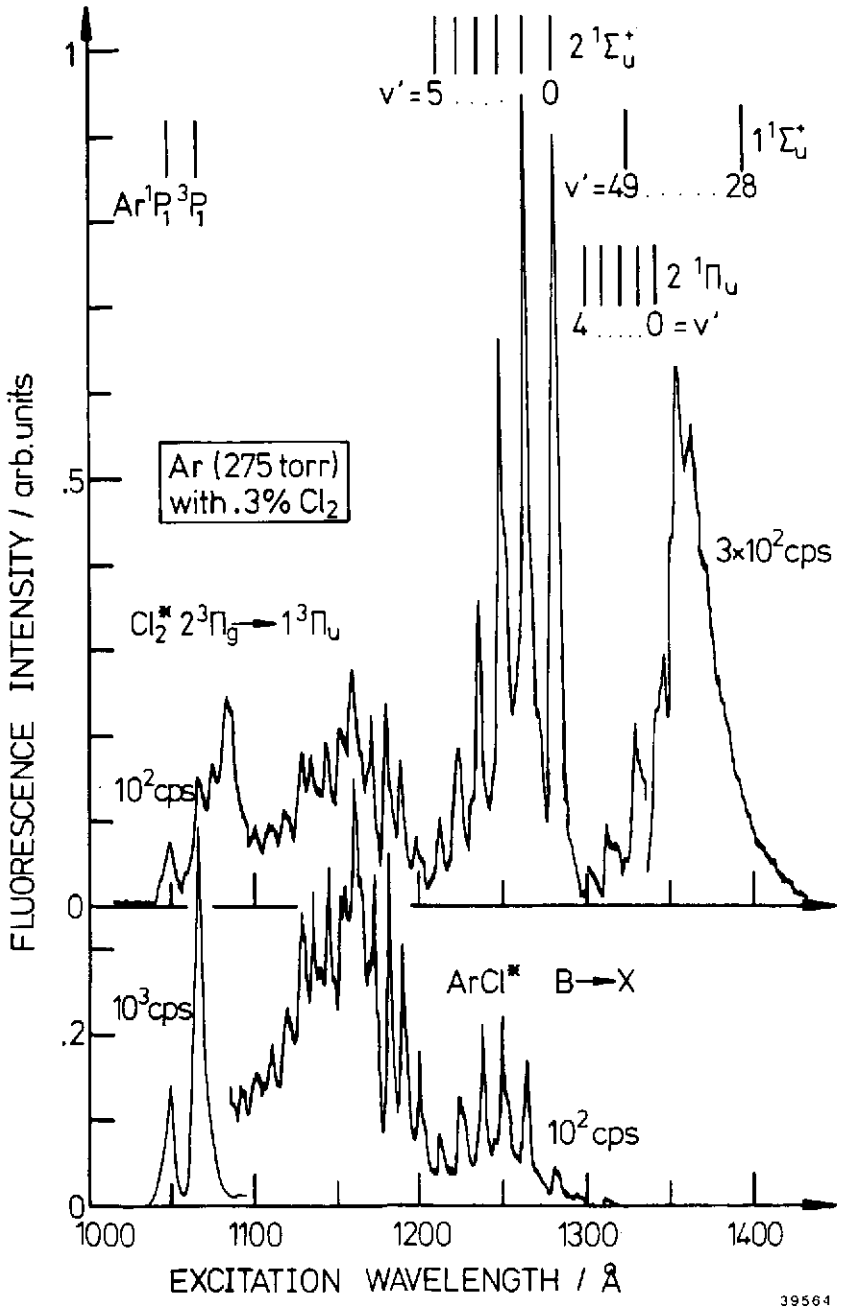
FLUORESCENCE INTENSITY / arb.units
1
.5
0
.2
0
$2\,^1\Sigma_u^+$
v'=5 0
$1\,^1\Sigma_u^+$
v'=49 28
$2\,^1\Pi_u$
4 . . . . . 0 = v'
$Ar\,^1P_1\,^3P_1$
Ar (275 torr)
with .3% Cl_2
3×10^2cps
$Cl_2^*\,2\,^3\Pi_g \rightarrow 1\,^3\Pi_u$
10^2cps
10^3cps
ArCl* B→X
10^2cps
1000
1100
1200
1300
1400
EXCITATION WAVELENGTH / Å
39564

Fig. 3

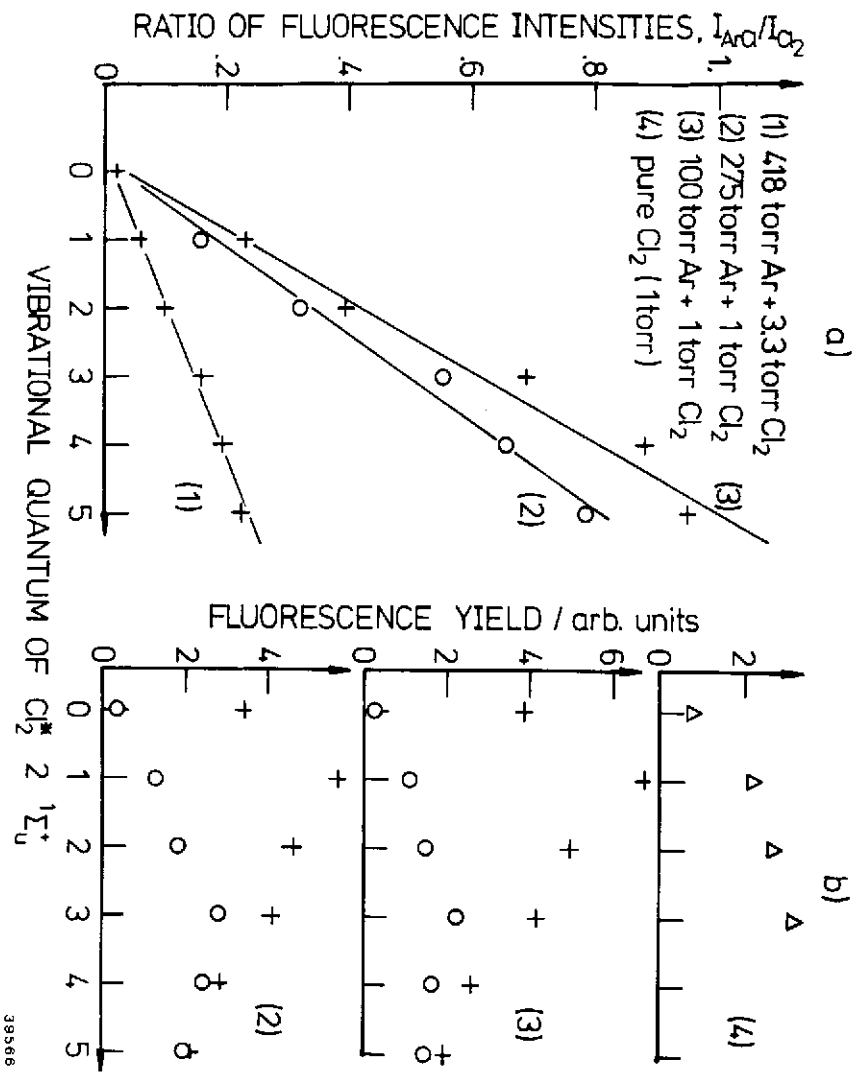
RATIO OF FLUORESCENCE INTENSITIES, I_{ArCl}/I_{Cl_2}
0
.2
.4
.6
.8
1.
(1) 418 torr Ar + 3.3 torr Cl_2
(2) 275 torr Ar + 1 torr Cl_2
(3) 100 torr Ar + 1 torr Cl_2
(4) pure Cl_2 (1 torr)
a)
VIBRATIONAL QUANTUM OF $Cl_2^*\,2\,^1\Sigma_u^+$
0 1 2 3 4 5
(1)
(2)
(3)
FLUORESCENCE YIELD / arb. units
0 2 4
0 2 4 6
0 2
(2)
(3)
(4)
b)
39566

Fig. 4

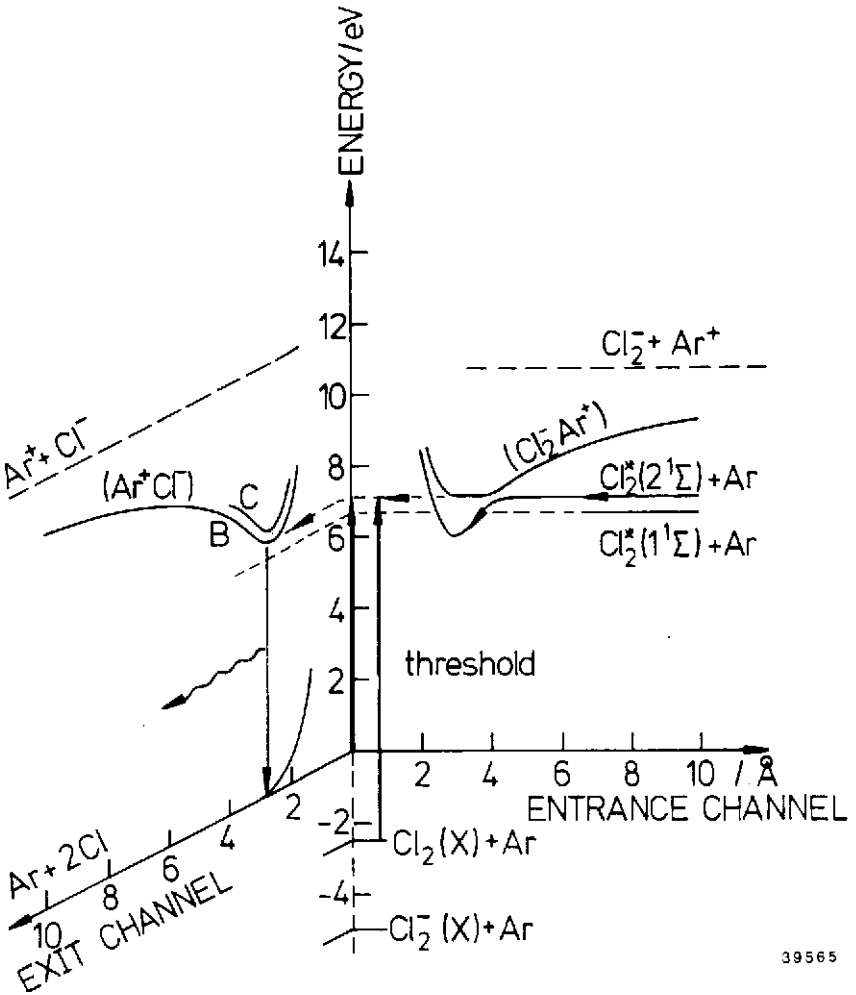
ENERGY/eV
14
12
10
8
6
4
2
-2
-4
$Cl_2^- + Ar^+$
$Ar^+ + Cl^-$
(Ar^+Cl^-)
C
B
$(Cl_2^-Ar^+)$
$Cl_2^*(2^1\Sigma) + Ar$
$Cl_2^*(1^1\Sigma) + Ar$
threshold
2 4 6 8 10 / Å
ENTRANCE CHANNEL
$Cl_2(X) + Ar$
$Cl_2^-(X) + Ar$
Ar + 2Cl
2 4 6 8 10
EXIT CHANNEL
39565

Fig. 5

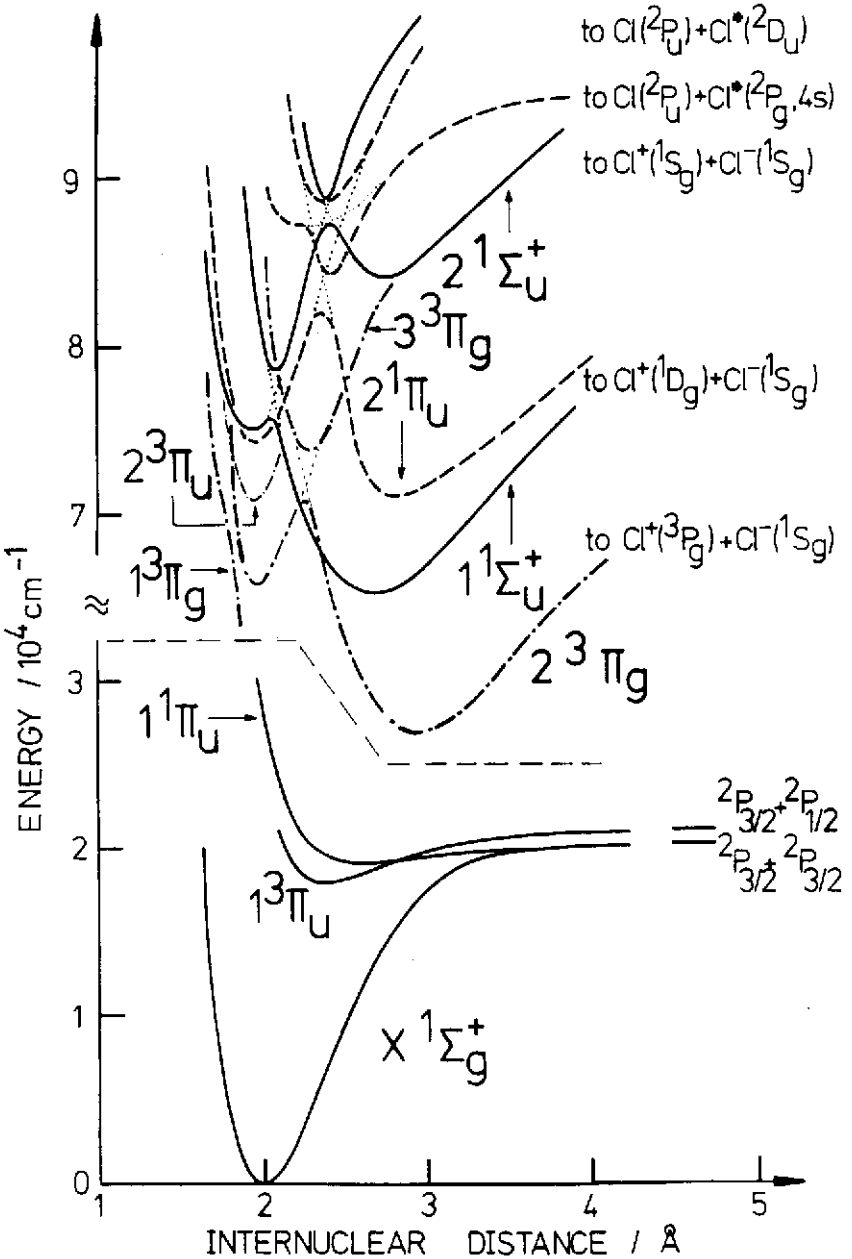
to $Cl(^2P_u) + Cl^*(^2D_u)$
to $Cl(^2P_u) + Cl^*(^2P_g, 4s)$
to $Cl^+(^1S_g) + Cl^-(^1S_g)$
$2^1\Sigma_u^+$
$3^3\pi_g$
$2^1\pi_u$
to $Cl^+(^1D_g) + Cl^-(^1S_g)$
$2^3\pi_u$
$1^3\pi_g$
$1^1\Sigma_u^+$
to $Cl^+(^3P_g) + Cl^-(^1S_g)$
$2^3\pi_g$
$1^1\pi_u$
$^2P_{3/2} + ^2P_{1/2}$
$^2P_{3/2} + ^2P_{3/2}$
$1^3\pi_u$
$X^1\Sigma_g^+$
ENERGY / 10^4 cm^{-1}
9
8
7
3
2
1
0
1 2 3 4 5
INTERNUCLEAR DISTANCE / Å
39561

Fig. 6

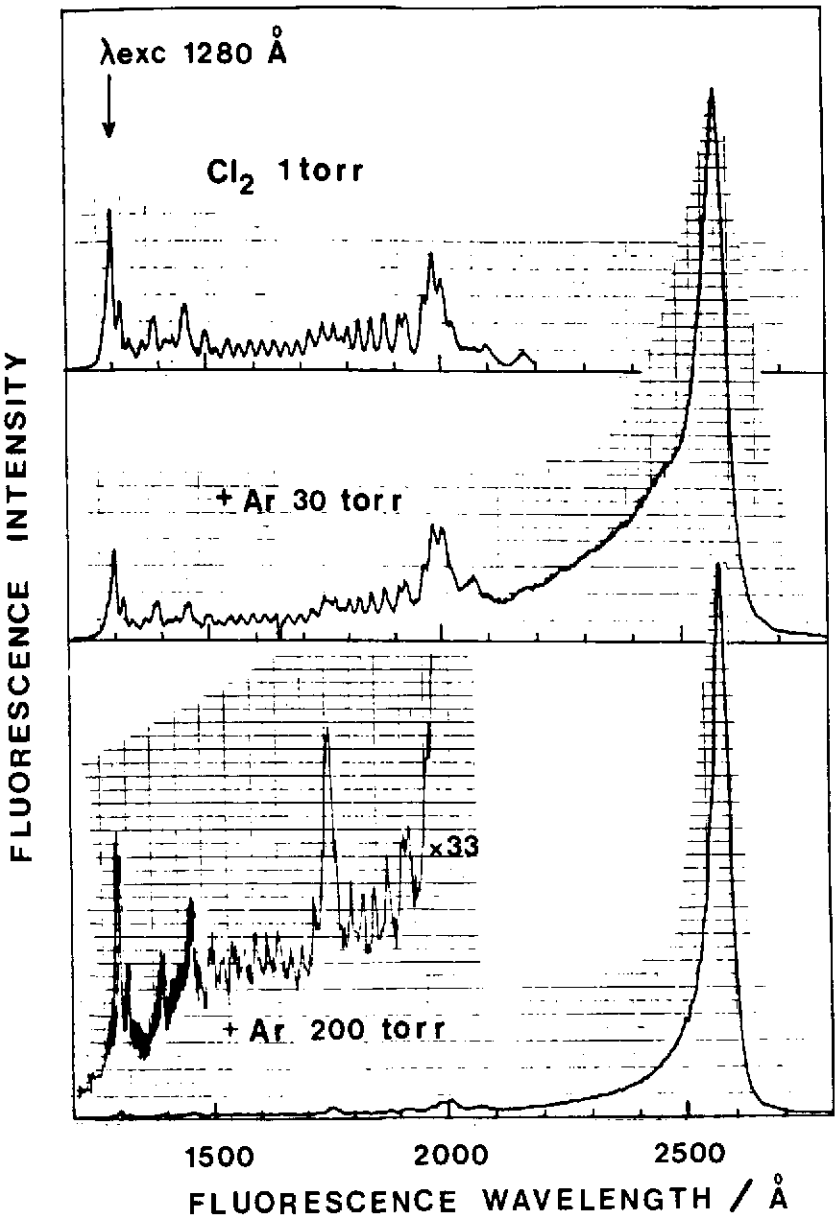
λexc 1280 Å
Cl2 1 torr
+ Ar 30 torr
x33
+ Ar 200 torr
FLUORESCENCE INTENSITY
1500
2000
2500
FLUORESCENCE WAVELENGTH / Å

Fig. 7

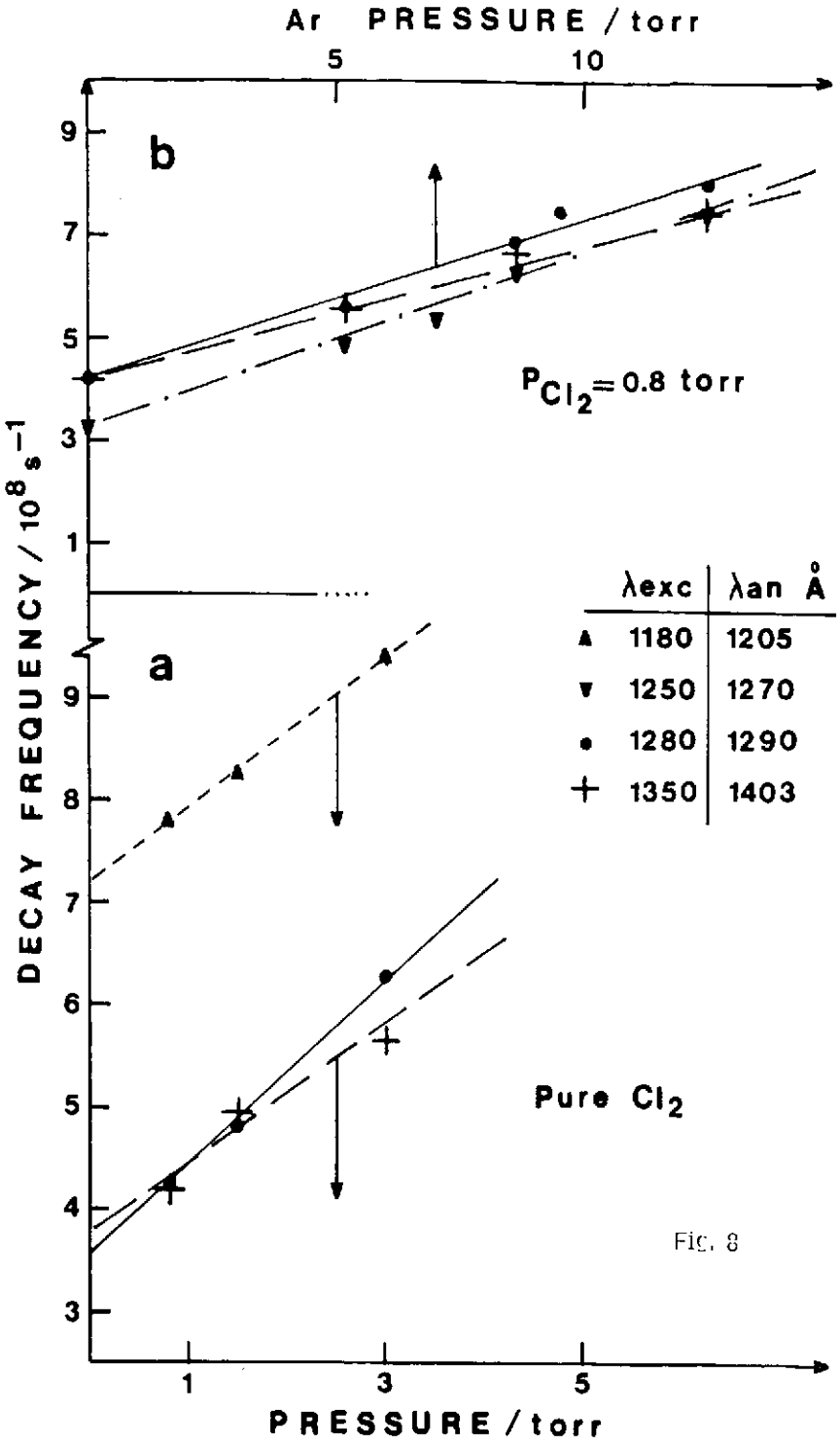
Ar PRESSURE / torr
5
10
b
P Cl2 = 0.8 torr
a
Pure Cl2
DECAY FREQUENCY / 10^8 s^-1
λexc | λan Å
1180 | 1205
1250 | 1270
1280 | 1290
1350 | 1403
1
3
5
PRESSURE / torr

Fig. 8

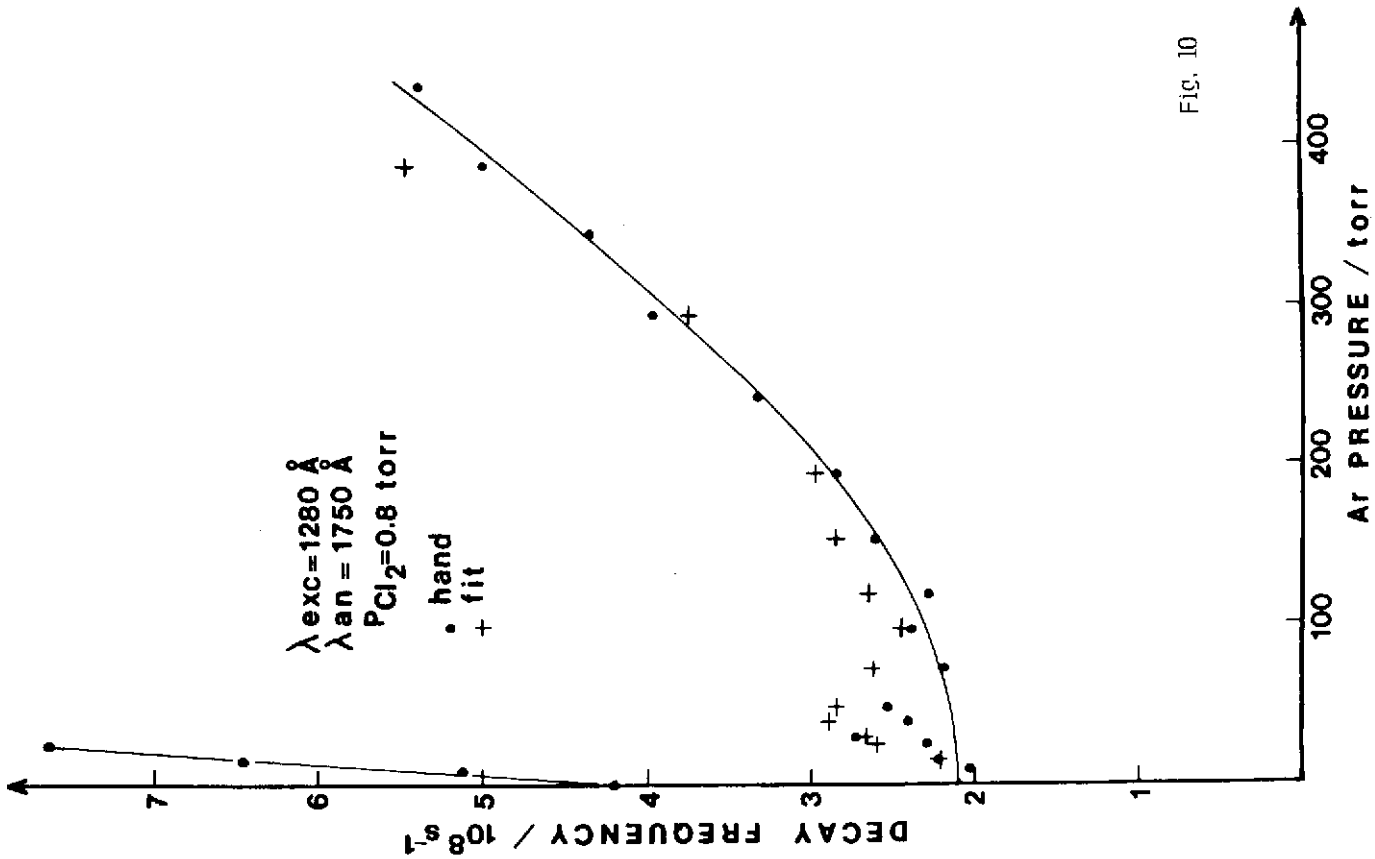
λexc=1280 Å
λan = 1750 Å
P_{Cl_2}=0.8 torr
• hand
+ fit
DECAY FREQUENCY / $10^8 s^{-1}$
Ar PRESSURE / torr
100
200
300
400
1
2
3
4
5
6
7

Fig. 10

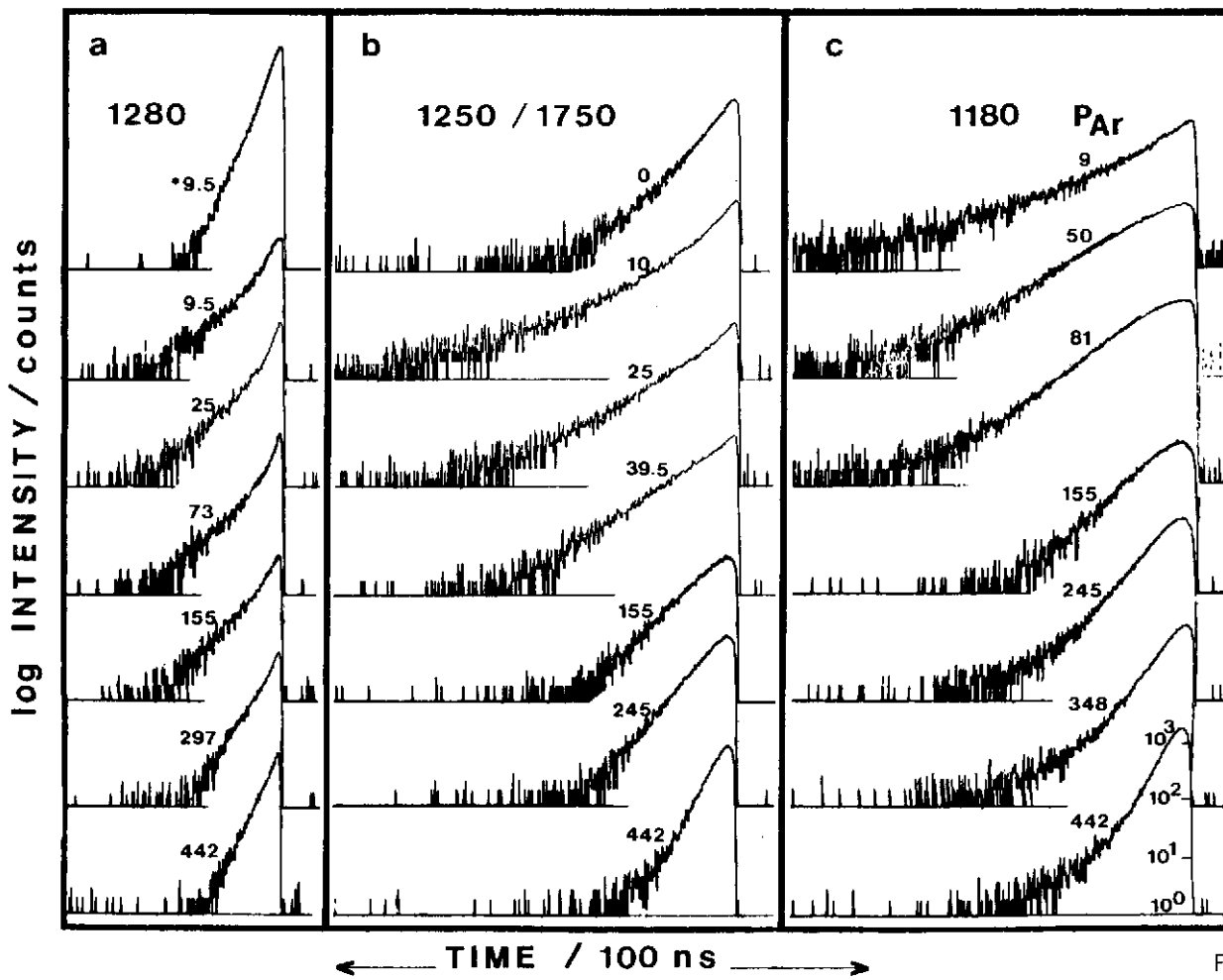
a
1280
*9.5
9.5
25
73
155
297
442
b
1250 / 1750
0
10
25
39.5
155
245
442
c
1180
P_{Ar}
9
50
81
155
245
348
10^3
10^2
10^1
10^0
log INTENSITY / counts
TIME / 100 ns

Fig. 9

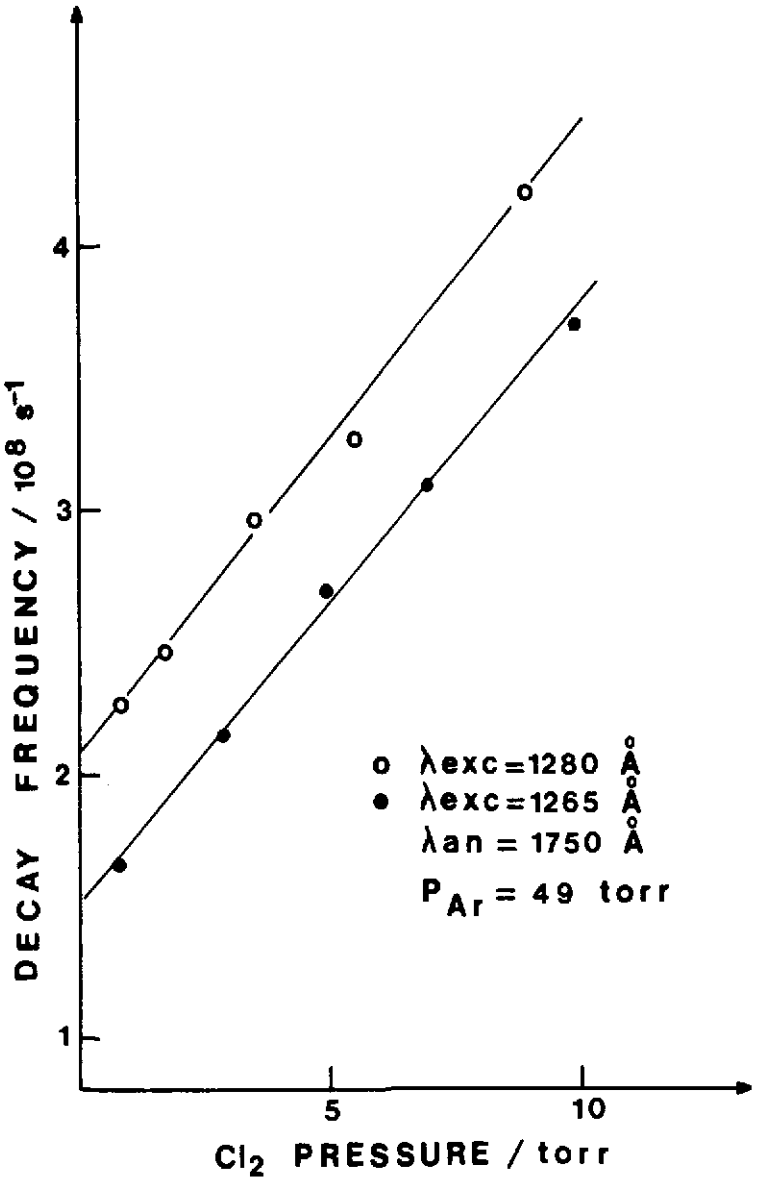
DECAY FREQUENCY / 10^8 s^{-1}
1
2
3
4
5
10
Cl_2 PRESSURE / torr
o λexc=1280 Å
• λexc=1265 Å
λan = 1750 Å
P_{Ar} = 49 torr

Fig. 11

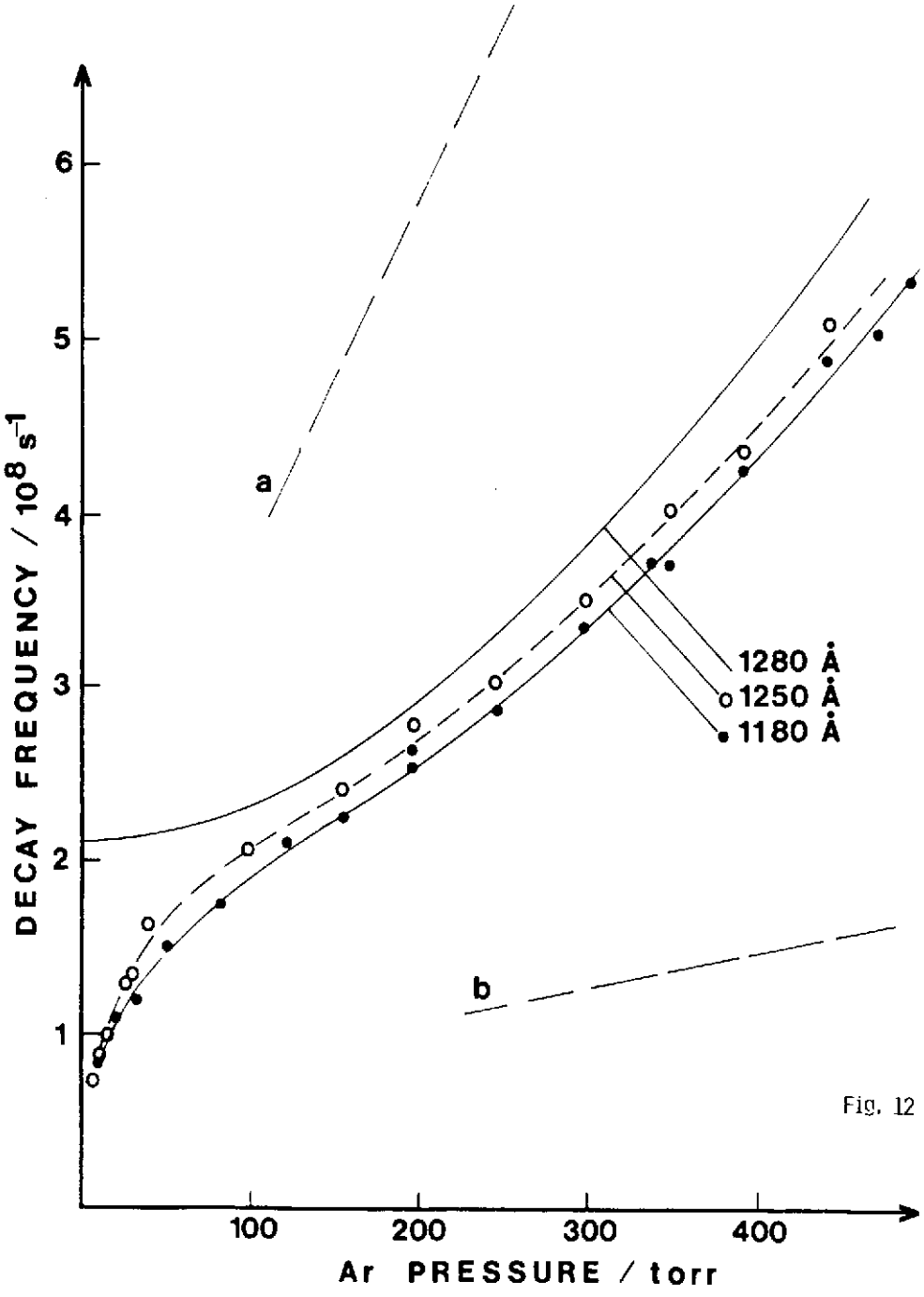
DECAY FREQUENCY / 10^8 s^{-1}
1
2
3
4
5
6
100
200
300
400
Ar PRESSURE / torr
a
b
1280 Å
1250 Å
1180 Å

Fig. 12

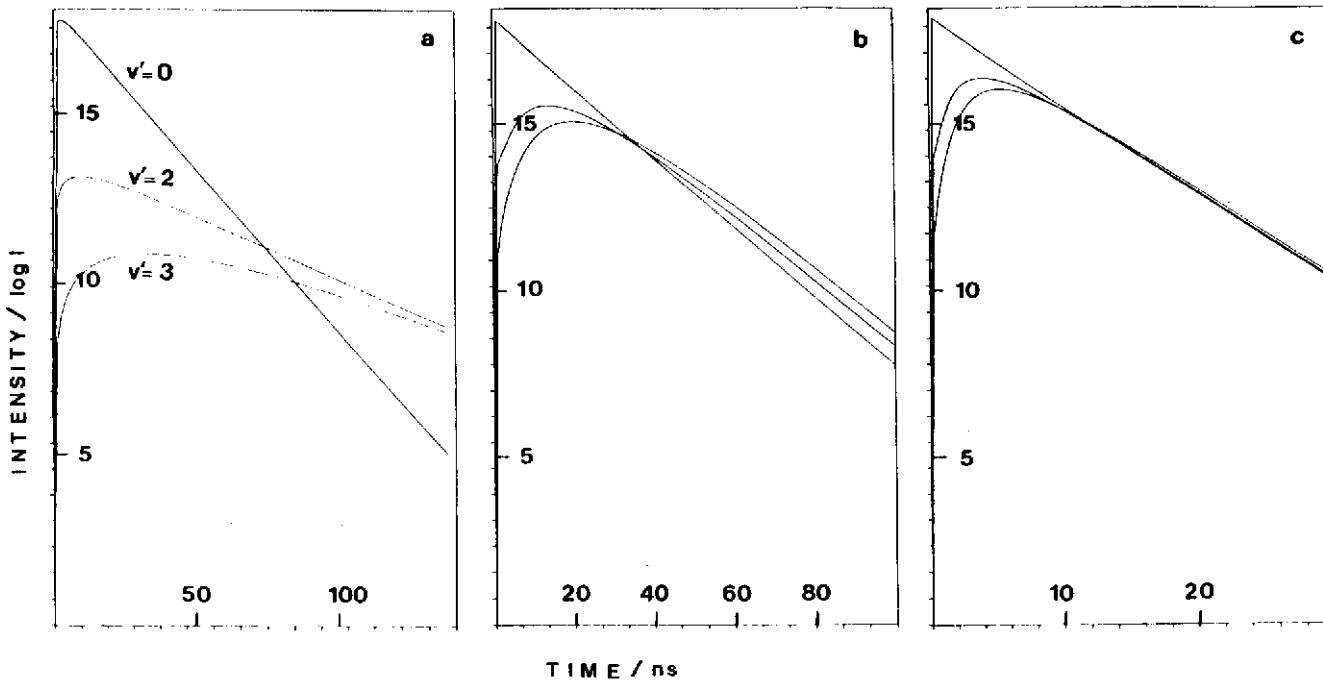
a
b
c
v'=0
v'=2
v'=3
15
10
5
50
100
20
40
60
80
10
20
INTENSITY / log I
TIME / ns

Fig. 12

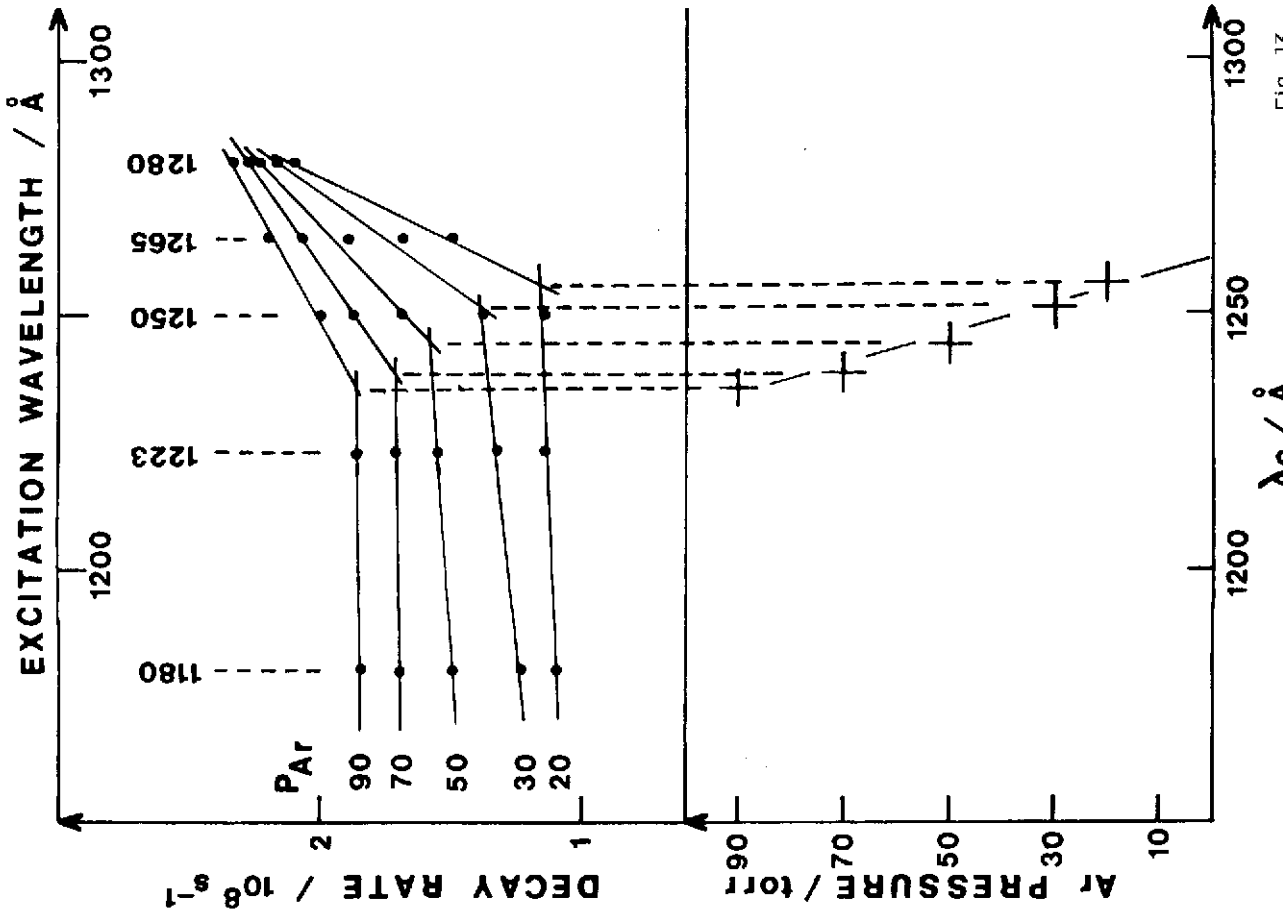
EXCITATION WAVELENGTH / Å
1300
1200
1280
1265
1250
1223
1180
P_Ar
90
70
50
30
20
DECAY RATE / 10^8 s^-1
2
1
Ar PRESSURE / torr
90
70
50
30
10
λc / Å
1300
1250
1200

Fig. 13

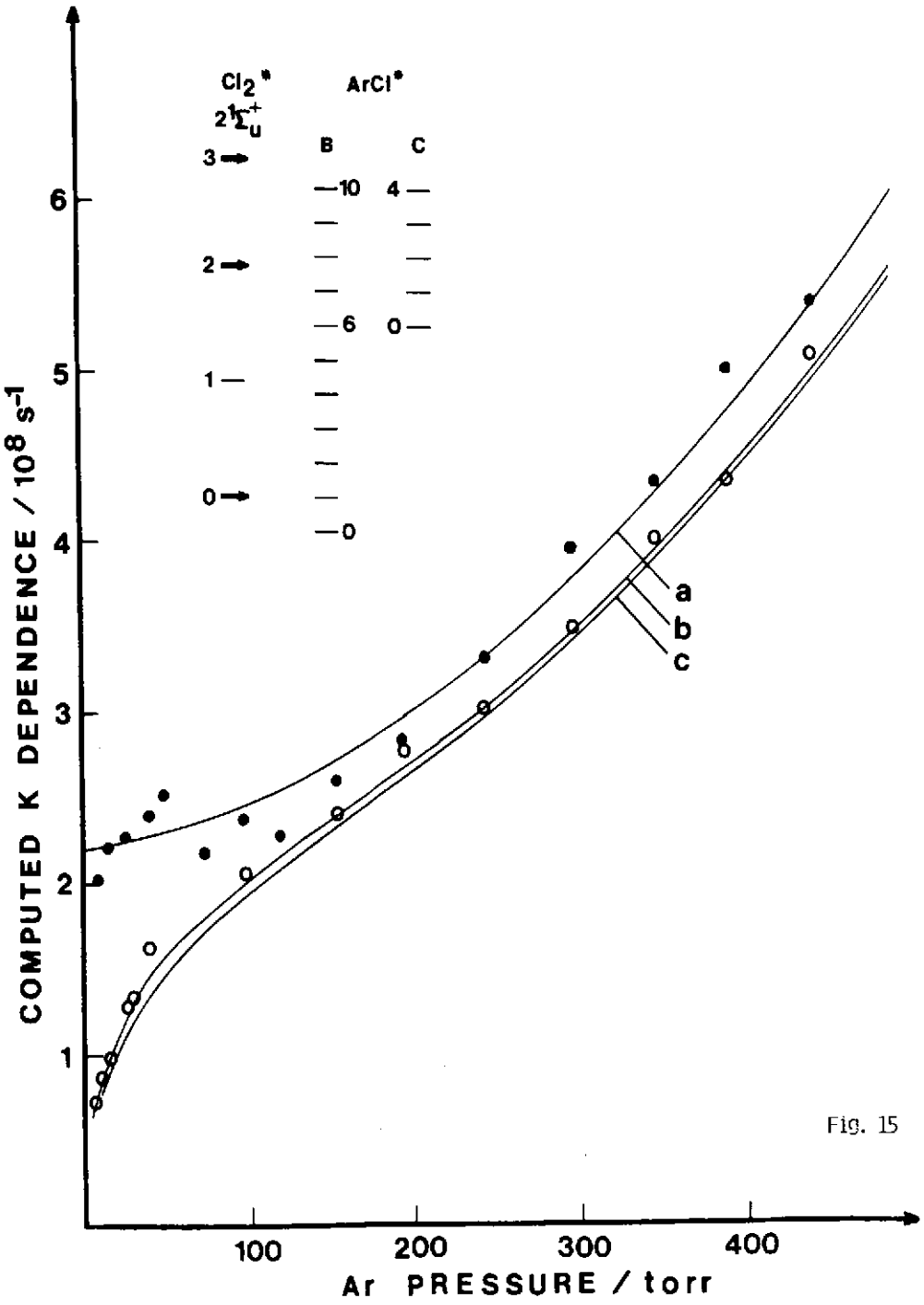
Cl_2^*
$2^1\Sigma_u^+$
ArCl*
B
C
3
2
1
0
10
6
0
4
0
a
b
c
COMPUTED K DEPENDENCE / 10^8 s^{-1}
Ar PRESSURE / torr
100
200
300
400
1
2
3
4
5
6

Fig. 15